Design and Calibration of Water-Cooled Calorimeter for Induction Motors

Shayan Daryabin

School of Electrical Engineering

Thesis submitted for examination for the degree of Master of Science in Technology.

Espoo 26.11.2018

Supervisor

Prof. Antero Arkkio

Advisor

Devi Geetha Nair(MSc)

Aalto University
School of Electrical
Engineering

Aalto University
School of Electrical
Engineering

Aalto University, P.O. BOX 11000, 00076 AALTO
www.aalto.fi
Abstract of the master's thesis

Author Shayan Daryabin

Title Design and Calibration of Water-Cooled Calorimeter for Induction Motors

Degree programme Automation and electrical engineering

Major Electrical Power and Energy Engineering **Code of major** ELEC3024

Supervisor Prof. Antero Arkkio

Advisor Devi Geetha Nair(MSc)

Date 26.11.2018 **Number of pages** 55+1 **Language** English

Abstract

A balanced water-cooled calorimeter is designed and implemented for electromagnetic power loss measurement of a 37 kW induction motor. The electromagnetic losses of the induction motor are measured at different loads and no-load.

In order to meet the IEEE 841 Standard, the ambient temperature for the test motor must not exceed 40 °C. The efficiency for the test motor is 92%, and it is expected the upper limit for the power loss of the test motor is not higher than 3.7 kW. It is approved, the calorimeter is feasible to measure power loss up to 4 kW, while the air temperature in the chamber, near to the test object, is less than 40 °C.

Two calibration curves, one with $2\frac{\mathrm{L}}{\mathrm{min}}$ and another one with $5\frac{\mathrm{L}}{\mathrm{min}}$ cooling flow rate are made conducted with a balance heater for the 37 kW induction motor. The first calibration curve is assigned for the total loss up to 2.5 kW and the latter for losses ranging from 2.5 to 4 kW. Using the calibration curves, reduce the balanced calorimetric measurement by almost 6 hours.

A heat-compensation method for the shaft heat-leakage is suggested and employed when the test motor is coupled with a loading machine. Experiments at no-load show the highest heat-leakage is due to the shaft heat-leakage. The uncertainty of the calorimetric measurement is 2.4% when the load torque is 201 Nm.

Keywords Calorimetry, induction motors, measurement techniques, power measurement

Preface

It was a great honour to do my master thesis under the supervision of Prof. Antero Arkkio and I would like to thank my advisor Devi Geetha Nair for entrusting me with this work. I am grateful to Ari Haavisto for his essential help and contribution in implementing the calorimeter system. I appreciate all my friends in the Aalto University Research Group of Electromechanics for making a friendly workplace. Lastly but more importantly, I am genuinely thankful for my lovely parents and my bother for their love, support and encouragement.

Otaniemi, 26.11.2018

Shayan Daryabin

Contents

Symbols and Abbreviations

Symbols

α	Temperature coefficient of a material
α	Uniform distribution of error
η	Efficiency
ΔQ_b	Rate of thermal energy during balance test
ΔQ_in	Absolute error in input power
ΔQ_loss	Absolute error in total power
ΔQ_out	Absolute error in output power
ΔQ_t	Rate of thermal energy during actual test
ΔT	Temperature difference
ΔT_max	Maximum temperature rise
Θ	Temperature
Θ_amb	Ambient temperature
$\overline{\Theta_\mathrm{Cham}}$	Chamber's average temperature
Θ_0	Temperature at initial time
Θ_∞	Temperature at infinite
λ	Thermal conductivity
ρ	Conductor resistivity
ρ	Density
ρ_0	Conductor resistivity at reference temperature
σ	Material conductivity
τ_th	Thermal time constant
ω	Angular frequency
a	Number of turns of a winding
A	Surface area
C_p	Specific heat capacity
$C_\mathrm{p,air}$	Specific heat capacity of air
$C_\mathrm{p,W}$	Specific heat capacity of water
d	Width
I	Stator line current
I_Ph	Stator phase current
I_r	Rotor current per phase
I_t	Test current
K	Thermal conductivity
K_Ru	Resistance factor
L	Length of thermal conductor
l_c	Length of winding
M	Torque
N_r	Mechanical rotor speed
N_s	Synchronous speed
P_c	Constant losses

P_{Cable}	Cable loss
P_{coolant}	Coolant power
P_{em}	Electromagnetic loss
P_{fe}	Core losses
P_{fw}	Friction and windage losses
$P_{\text{fan,hex}}$	Heat-exchanger fan's loss
$P_{\text{fan,res}}$	Balance heater's fan loss
P_{in}	Input power
$P_{\text{in,s}}$	Input power to the motor while the rotor is removed
P_{loss}	Total motor loss
P_{m}	Mechanical power to drive the rotor without applied voltage to the stator
P_{mech}	Mechanical output power
P_{nl}	No-load power loss
P_{out}	Output power
P_{r}	Rotor loss
P_{rr}	Input power during the rotor reverse test
P_{res}	Balance heater loss
P_{s}	Stator loss
P_{SL}	Stray load losses
P_{SLr}	High frequency stray load losses
P_{SLs}	Fundamental stray losses
P_{sn}	Stator windings losses at no-load
P_{total}	Total power loss
P_{vent}	Ventilation loss
P_{W}	Power absorbed by water
P_{wall}	Wall heat-leakage
Q	Heat
$\dot{Q}$	Rate of heat transfer
$\dot{Q}_{\text{air}}$	Rate of thermal energy of air
$\dot{Q}_{\text{W}}$	Rate of thermal energy of water
q_{b}	Total heat-leakage during the balance test
$q_{\text{b-holes}}$	Heat-leakage of holes during the balance test
$q_{\text{b-shaft}}$	Heat-leakage of shaft during the balance test
$q_{\text{b-walls}}$	Heat-leakage of walls during the balance test
q_{cond}	Shaft heat-leakage due to the conduction at 5 $\frac{\text{L}}{\text{min}}$
q'_{cond}	Shaft heat-leakage due to the conduction at 2 $\frac{\text{L}}{\text{min}}$
q_{t}	Total heat-leakage during actual test
R	Resistance of a conductor
R_{AC}	AC resistance of stator
R_{DC}	DC resistance of stator
R_{r}	Rotor resistance
R_{t1}	Stator resistance at $\text{t}_1 temperature$
R_{t2}	Stator resistance at $\text{t}_2 temperature$
S	Surface area
s_{a}	Slip at temperature t_{a}

s_b	Slip at the specified temperature t_b
S_c	Cross section area of a conductor
T	temperature
t_b	Specified temperature
T_in	Inlet water temperature
$T_\mathrm{in,Max}$	Maximum input temperature
$T_\mathrm{in,Min}$	Minimum input temperature
T_K	Conductivity expressed as varying percentage of IACS
T_o	Outlet water temperature
T_r	Temperature rise
T_0	Reference temperature for a conductor
T_1	Shaft temperature before passing the wall
T_2	Shaft temperature after insulation
$\dot{V}$	Water flow rate

Abbreviations

AC	alternating current
DC	direct current
IACS	International annealed copper standard
IE	International efficiency
Pt	Platinum
SynRM	Synchronous reluctance motor

List of Figures

List of Tables

1 Introduction

The dissipated heat of the electric motors are equivalent to their power losses, and a calorimeter measures the loss or the the generated heat produced by the electric motors directly. The uncertainty of measurement in input-output method, the most common power loss measurement method, is high and not satisfactory at high efficient motors. Worth mentioning, there is no standard method to determine the efficiency for SynRM and other machines fed by converter[1]. In addition, it is estimated that electric motor- driven systems account for between 43% and 46% of all global electricity consumption[2]; therefore, electric motors are regarded as one of the most significant loads in the grid. So, it is beneficial and necessary to study and implement other methods to verify the power loss measurements of the electric motors.

Unlike the input-output method, the calorimetry is not dependent on efficiency and the power range of the electric motors. Open-cycle air cooled calorimeters are the most common calorimeters utilized for loss measurement of the electric motors due to its simple structure and shorter response time comparing to the other types of the calorimeters. However, air as coolant has more variation in heat capacity and density at different temperatures comparing to water. Water is used as coolant in the designed balanced calorimeter.

Thesis structure

- **Chapter 2** Literature review of the losses and approaches to measure and calculate the loss components of the induction motors.
- **Chapter 3** Literature review of the input-output and calorimetry methods for loss measurements, and study the classification of the calorimeters.
- **Chapter 4** Outline the structure of the balanced calorimeter, and principle of the calorimeteric measurements.
- **Chapter 5** Experiments to verify the balanced calorimeter while construction
- **Chapter 6** Outline the calorimetric and input-output measurement results for the 37 kW induction motor
- **Chapter 7** Conclusions based on the observations and results, and new suggestions for the water circuit of the water-cooled calorimeters

Objectives

- Design, construct and calibrate the balanced water-cooled calorimeter for the 37 kW induction motor
- Measure the electromagnetic losses of the 37 kW induction motor throught the calorimeter

2 Losses in Induction Motors

Total loss in the induction motors are divided into two groups of constant and load losses[3]. The first includes the core and friction and windage losses which are not varied by the load, and the latter includes stator and rotor winding losses and stray losses which are increased by the load increment. The core and the friction and windage losses can be measured based on the no-load test [4].

2.1 Stator Winding Losses

The stator winding losses are due to the resistive copper losses[5]. The resistance of each phase of the 37 kW induction motor is measured at stand still through four wire method [6]. The DC resistance of the motor can be measured, using a current source and a voltmeter [7]. The resistive stator winding losses increase due to the temperature rise at full load. The dc resistance at the steady state temperature can be expressed as:

$$R_{t_2} = R_{t_1}(1 + \alpha(t_2 - t_1)) \tag{1}$$

where R_{t_2} is the stator resistance at steady state temperature, R_{t_1} is the DC stator resistance at stand still, and α is the temperature coefficient of copper. In addition, the dc winding resistance is relying on the total length l_c , number of turns of windings a, the cross section area of the conductor S_c, and the conductivity of the conductor material σ [8]. The DC winding resistance is expressed as:

$$R_{DC} = \frac{l_c}{\sigma_c a S_c} \tag{2}$$

In order to calculate the AC resistance, the DC resistance can be multiplied by a winding resistance factor k_{Ru}. The winding resistance factor depends on the dimension of a slot, dimension and number of subconductors in a slot [8].

$$R_{AC} = R_{DC} k_{Ru} \tag{3}$$

Stator winding losses increase due to the skin effect in the end windings and slots. Moreover, there are eddy current losses in the stator windings which are relying on the distance of the air gap to the windings and high frequency harmonics if the motor is fed by a frequency convertor [9] . The highest portion of losses, almost 41 % of total loss, takes place in the stator windings resistance in the cage induction motors [5] . The stator losses can be expressed as:

$$P_s = 3 R_{DC} I_{ph}^2 \tag{4}$$

where I_{ph} is the phase current in the stator windings.

2.2 Rotor Winding Losses

The squirrel cage rotor entails a cylindrical laminated steel core, and axial slots to carry the conductor bars, and the bars are connected to each other by the end rings [10] . The induced current flow produced by the fundamental flux in the rotor cage resistance including the bars and the end rings brings about the rotor or slip losses. The rotor losses or the slip losses can be expressed as [5] :

$$P_{\mathrm{r}} = 3R_{\mathrm{r}}I_{\mathrm{r}}^2 \tag{5}$$

where P_{r} is the rotor power loss,R_{r} and I_{r} are the total rotor resistance and the rotor current per phase respectively. The cage rotor resistance cannot be measured [5]. Alternatively, the rotor losses can be expressed:

$$P_{\mathrm{r}} = (P_{\mathrm{in}} - P_{\mathrm{s}} - P_{\mathrm{nl}})s \tag{6}$$

where P_{in} and $P_{\,rms}$ are the input and the resistive stator power losss at any load [5] , P_{nl} is power loss at no-load, and s is the slip. The slip can be can be calculated by the following equation:

$$s = \frac{N_{\mathrm{s}} - N_{\mathrm{r}}}{N_{\mathrm{s}}} \tag{7}$$

where N_{s} is the synchronous speed and N_{r} is the mechanical rotor speed. The slip may change by the temperature increment; hence, the slip is measured when the stator windings temperature reach the specified temperature according to the IEEE Std 112. The specified temperature is the measured temperature rise of a resistance at the rated load plus 25°C. Also, the specified temperature can be determined by the windings insulation class. The slip at the specified temperature can be expressed [11]:

$$s_{\mathrm{b}} = \frac{s_{\mathrm{a}}(t_{\mathrm{b}} + T_{\mathrm{k}})}{t + T_{\mathrm{k}}} \tag{8}$$

where s_{b} is the corrected slip at the specified temperature t_{b},s_{a} is the measured slip at the stator temperature t_{a},and T_{k} is 234.5 for 100% IACS conductivity of copper, and 225 for 62% IACS conductivity of aluminium.

2.3 Constant Losses

The constant losses are losses which are not varied by load; therefore, they can be determined by their no load values. The constant losses include core, friction and windage losses. The difference of the input power and the stator resistive losses at no-load test defines the constant losses.

$$P_{\mathrm{c}} = P_{\mathrm{in}} - P_{\mathrm{sn}} = P_{\mathrm{fw}} + P_{\mathrm{fe}} \tag{9}$$

Where P_{c} is the constant losses, P_{in} is the input power, P_{sn} is the stator windings resistive losses at no-laod, P_{fw} is the friction and windage losses, and P_{fe} is the core losses.

In order to estimate the friction and windage losses, the voltage must be reduced progressively from rated to a lowest voltage level at no-load, while the rotor runs at its rated speed. The power loss value which corresponds to the extrapolated power at zero voltage is regarded as the friction and windage losses in a curve made by the measured constant power losses points as a function of the squared voltage at no-load test[12]. The subtraction of the constant losses from the friction and windage losses when the voltage range is 90% to 110% of the rated voltage at no-load derives the core losses[12]. In addition to the no-load test at variable speed, there is a method called retardation test which also estimates the friction and windage losses in the electrical machines. In the latter test, the motor is supplied by a synchronous generator. The motor runs at no-load to stabilize the bearing temperature. Initially, the motor runs at a rotational speed slightly higher than the rated speed, then the test motor is disconnected from the synchronous supplier. During deceleration of the rotor, the rotational speed is measured and recorded progressively. A curve of speed as a function of time is plotted. The friction and windage loss can be estimated by having the time derivation of rotational speed and the moment of inertia of rotor[13].

2.4 Stray load losses

Stray load losses are parts of the total loss of the electric machines that are neglected in the stator, rotor, core, friction and windage losses. Stray load losses are due to current linkage harmonics, permeance harmonics produced by the stator windings, stator and rotor slots, and saturation harmonics in the core lamination[12]. It can be calculated indirectly as the following equation:

$$P_{\mathrm{SL}} = P_{\mathrm{in}} - P_{\mathrm{out}} - P_{\mathrm{s}} - P_{\mathrm{r}} - P_{\mathrm{fe}} - P_{\mathrm{fw}} \tag{10}$$

The stray load losses at fundamental frequency can be measured by a rotor removed test and applying balance voltage to the stator. The difference of a rotor removed input power and the I^2R stator losses describes the stray losses at fundamental frequency as the following equation :

$$P_{\mathrm{SLs}} = P_{\mathrm{in,s}} - P_{\mathrm{s}} \tag{11}$$

where $P_{\mathrm{in,s}}$ is the input power to the motor while the rotor is removed.

The stray load losses at high frequency can be measured by a reverse rotor test. The rotor is driven by an external mover at or near the synchronous speed at the opposite direction of the rotation of the stator magnetic field, and the input power is measured. In the rotor reverse test, the needed mechanical power to drive the motor is measured without current and with a test current. The high frequency stray loss component is expressed as :

$$P_{\mathrm{SLr}} = (P_{\mathrm{r}} - P_{\mathrm{m}}) - (P_{\mathrm{rr}} - P_{\mathrm{SLs}} - P_{\mathrm{in,s}}) \tag{12}$$

where P_{r} is the mechanical power required to drive the rotor in the opposite direction of the rotation of the magnetic field while a test current is applied to the stator, P_{m} is mechanical power to drive the rotor without applied voltage to the stator, P_{rr} is

the input power during the rotor reverse test. The test current for the two tests is defined as:

$$I_{\mathrm{t}} = \sqrt{(I^2 - I_0^2)} \tag{13}$$

where I_{t} is the test current at two tests,I^2 is stator line current at which the stray load loss is to be determined, and I_0 is the average of no load line currents at rated voltage. The summation of the fundamental and high frequency stray loss components indicate the stray load losses in the electrical machine.

$$P_{\mathrm{SL}} = P_{\mathrm{SLs}} + P_{\mathrm{SLr}} \tag{14}$$

3 Measurement Methods

3.1 Input-Output Method

The most common approach to measure the total loss of the electric motors is the input-output method. It can be expressed as [14]:

$$P_{\text{loss}} = P_{\text{in}} - P_{\text{mech}} \tag{15}$$

where P_{loss} is the total power loss,P_{in} is the active input power, and Pmech is the mechanical output power. A power analyser measures the electrical input power. The mechanical output power is expressed as:

$$P_{\text{mech}} = T_{\text{mech}}\omega \tag{16}$$

where T_{mech} is the mechanical output torque which is measured via a torque transducer, and ω is the rotational speed of the shaft. Efficiency is the ratio of the output to input power, and can be expressed by the three following equations[15]:

$$\eta = \frac{P_{\text{out}}}{P_{\text{in}}} \tag{17}$$

$$\eta = 1 - \frac{P_{\text{loss}}}{P_{\text{in}}} \tag{18}$$

$$\eta = \frac{1}{1 + \frac{P_{\text{loss}}}{P_{\text{out}}}} \tag{19}$$

Since 2009, for the squirrel cage induction motors with two, four and six poles, and rated power ranging from 0.75 to 375 kW three efficiency classes are proposed: 1) IE2-high efficiency 2) IE3-premium efficiency 3) IE4-super premium efficiency. Since 2017, all the motors ranging from 0.75 kW to 375 kW must meet IE3 efficiency class[16].

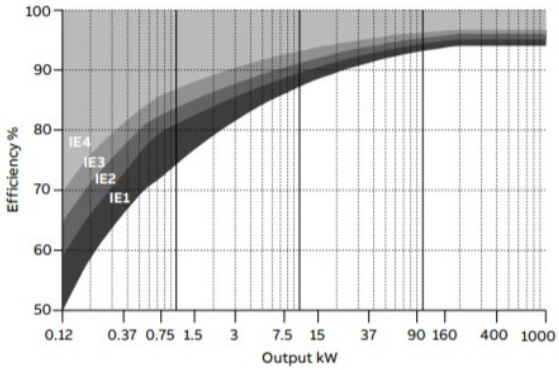

Figure 1: IE efficiency classes for 4-pole motors at 50 Hz[17]

Figure 1 shows the IE efficiency classes for four-poles motors at 50 Hz with respect to the output power.

The maximum relative error in the input-output method is expressed as[18]:

$$\left|\frac{\Delta P_{\text{loss}}}{P_{\text{loss}}}\right| < \frac{1}{1-\eta}\left(\left|\frac{\Delta P_{\text{in}}}{P_{\text{in}}}\right| + \left|\frac{\Delta P_{\text{out}}}{P_{\text{out}}}\right|\right) \tag{20}$$

where ΔP_{loss} is the absolute error in total power, ΔP_{in} is the absolute error in input power, and ΔP_{out} is the absolute error in output power .With the trends and the interests of increasing the efficiency in the motors, the maximum relative error for the total power loss measurement corresponding to the input-output method is relatively high.

3.2 Calorimetric Method

Calorimetric method is an approach to measure the power loss directly through the dissipated heat [19]. Hence, the power loss measurement in this method is not relying on the efficiency and the power range of the electric motors[20]. Figure 2 illustrates

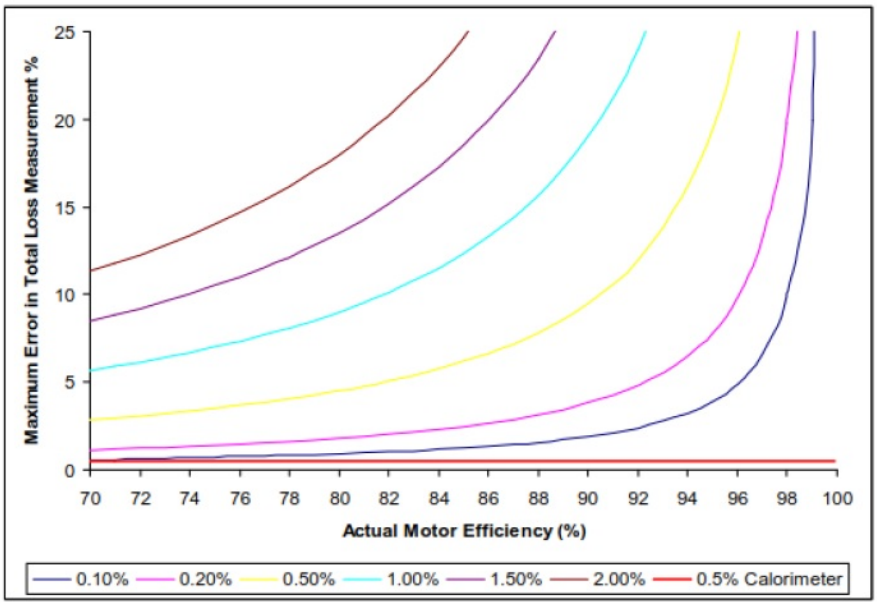

Figure 2: Comparison of calorimeter and input-output methods due to measurement errors [21]

the calorimeter's relative error is not changing by the efficiency variations, while the more efficient motors lead to more uncertainty in the power loss measurement in the input-output method. In addition, Figure 2 illustrates the maximum relative error of the input-output method at various instrumentation accuracies.

The induction motor or the test object is placed in an enclosed chamber, and a coolant flows into the chamber, absorbs the heat produced by test object, and flows out. The coolant power in the steady state is equivalent to the power loss of the test object, and can be expressed as:

$$P_{\text{coolant}} = \dot{V}(C_{\text{p2}}\rho_2 T_2 - C_{\text{p1}}\rho_1 T_1) = P_{\text{loss}} \tag{21}$$

where $\dot{V}$ is the volumetric flow rate in $\frac{\mathrm{m}^3}{s}$, C_p is the specific heat capacity in $\frac{\mathrm{J}}{\mathrm{Kg}^\circ\mathrm{C}}$, ρ is the density in $\frac{\mathrm{K}}{\mathrm{m}^3}$, and T is the temperature in °C of the coolant. Subscripts 1 and 2 refer to the entry and exhaust of the chamber respectively. If the heat capacity and density of the coolant are constant at the entry and the exhaust of the chamber, the coolant power is expressed as:

$$P_{\text{coolant}} = \dot{V}(C_\mathrm{p}\rho\Delta T) = P_{\text{loss}} \tag{22}$$

3.3 Classification of Calorimeters

Generally speaking, calorimeters are divided in two groups. First, direct calorimeter which measures the produced heat by the test object directly. Second, indirect calorimeter which is conducted by a reference heater, and the calorimeter determines the input power of the reference heater which produces the same temperature rise in the coolant as the test object. The input power of the reference heater represents the power loss in the test object. There are two types of direct calorimeters, gas-cooled open calorimeter and fluid-cooled closed calorimeter. Furthermoer, The indirect calorimeter is divided into two types. They are called balanced calorimeters and series calorimeters respectively.

3.3.1 Gas-Cooled Open Calorimeter

The coolant for the open calorimeter is gas, usually air. The air absorbs the produced heat of the test object with low response time[22]. Also, it has a simple structure, and a heat-exchanger is not needed[23]. Nevertheless, the air properties such as heat capacity and density significantly change with the variation of pressure, temperature and humidity which bring about variation in the thermal energy of the coolant; therefore, high precision, expensive instruments and temperature equalizers are necessary for accurate power loss measurements[23]. [22] designed a gas-cooled open calorimeter for electrical machines rated up to 300 kW with 0.2% uncertainty. Figure 3 illustrates the open calorimeter.

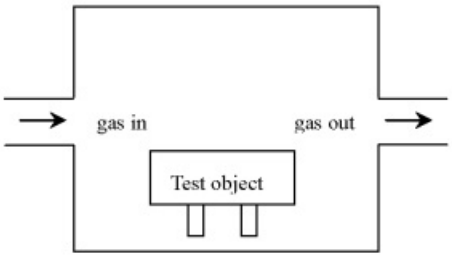

Figure 3: Direct: open calorimeter[19]

3.3.2 Liquid-Cooled Closed Calorimeters

Usually water is used as a coolant in the liquid-cooled, closed calorimeters. Water heat capacity and density change less than those of air with respect to temperature and pressure . In this type of calorimeter, first, the generated heat is transferred to the air, then the air heat is transferred to the water through a heat-exchanger and fans; therefore, the presence of the heat-exchanger is neccessary in this type of the calorimeter, since the coolant passes in the calorimeter via the heat-exchanger. The response time of the liquied-cooled calorimeter is longer than the air-cooled calorimeter due to the mentioned heat transmission processes. Nevertheless, the accuracy of the heat measurement in the water cooled calorimeter is higher than the air cooled type due to less variation of water properties such as heat capacity and density at different temperatures and higher thermal conductivity of water.

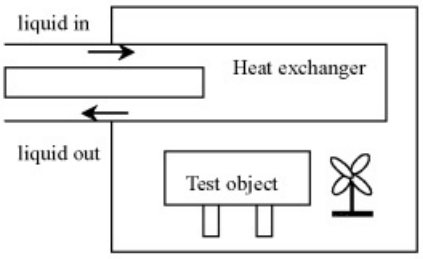

Figure 4: Direct: closed calorimeter[19]

3.3.3 Balanced Calorimeters

Two tests are employed in this type of calorimeters. The first test is conducted with the test object, and the second one is conducted with a reference heater. If the mass flow of the coolant and the heat-leakage are equal, the active input power for a reference heater which produces the same temperature rise in the coolant as the test object, represents the power loss of the test object. Hence, balanced calorimeter eliminates the need for accurate measurement of the coolant properties. Nevertheless, having two tests prolongs the duration of the power loss measurement in the balanced calorimeters. Furthermore, the assumption of the equal heat-leakage in the two test could not be true, as the dimensions of the reference heater and the test object are not equal, and they have different heat distributions. Figure 5 illustrates the balanced calorimeter. [24] reports a designed air cooled balance calorimeters for a 37 kW induction motor for maximum power loss up to 3 kW with 0.4 % uncertainty of measurement.

3.3.4 Series Calorimeter

Series calorimeter is also called double-chamber calorimeter, since two similar chambers are connected to each other. In this configuration, one chamber contains the

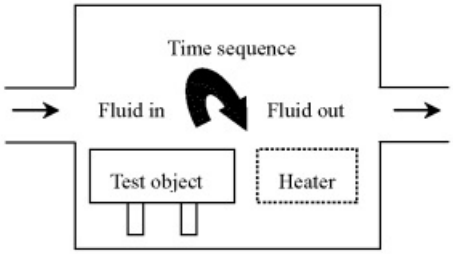

Figure 5: Indirect: balanced calorimeter[19]

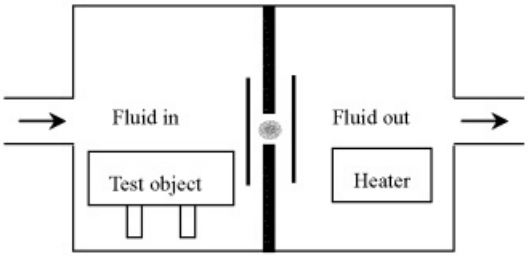

Figure 6: Indirect: series calorimeter[19]

test object, and the latter contains the reference heater. First, the coolant passes through the chamber where the test object is placed, then coolant passes through the second chamber where the reference heater exists. The input power of the reference heater is controlled and set to reach the same temperature rise in the coolant as the first chamber where the test object is placed. Like the balanced calorimeter, series calorimeter eliminates the need of accurate measurement of the coolant properties, as the active input power is regarded as the power loss of the test object. Also, the duration of calorimetric measurement is reduced by half comparing to the balanced calorimeter. Nevertheless, the heat-leakage in the two chambers would not be the same, since not only the reference heater and test object may not have the same heat distribution, but also the coolant temperature is not the same in the two chambers; hence, the coolant properties in the two chambers are not the same. Figure 6 illustrates the series calorimeter. [25] reports a series air-cooled calorimeter designed for a 7.5 induction motor and power loss up to 1 kW with 1.5% uncertainty.

4 Calorimetric Experimental Setup

In a water-cooled calorimeter, the heat is transferred to air from the test motor, then from air to water through the heat-exchanger. In steady state, the thermal energy of water and air are equivalent as it is shown in the following equations if the effectiveness of the heat-exchanger is unity, and the heat completely transfers from air to water. Effectiveness indicates the heat-exchanger's performance.

$$\dot{Q}_{\text{air}} = \dot{Q}_{\text{W}} \tag{23}$$

$$\dot{V}_{\text{air}}\rho_{\text{air}}C_{\text{p,air}}\Delta T_{\text{air}} = \dot{V}_{\text{W}}\rho_{\text{W}}C_{\text{p,W}}\Delta T_{\text{W}} \tag{24}$$

In equations 23 and 24, subscript W represents water. Figure 7 illustrates the top

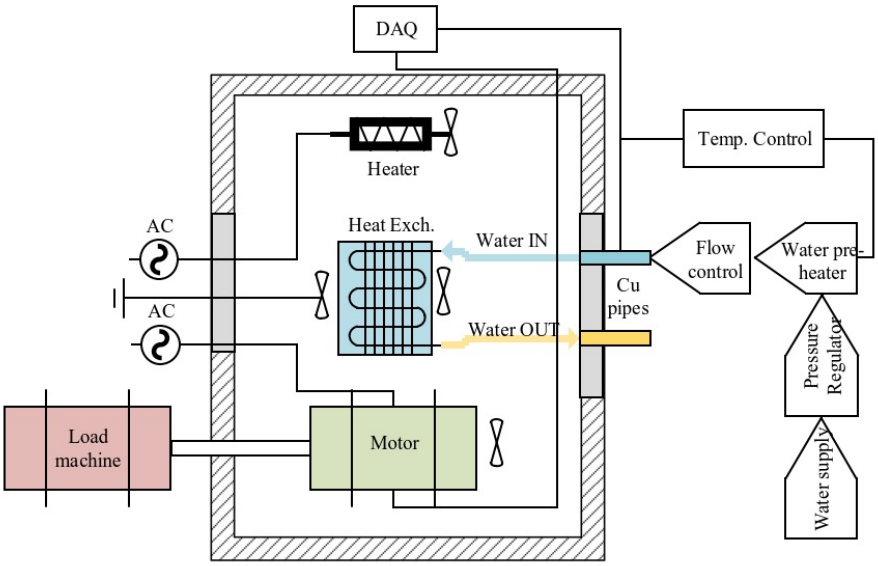

Figure 7: Top view of the water-cooled balance calorimeter layout[26]

view of the water-cooled balanced calorimeter, the layout includes the test motor, the loading machine, reference heater, water control circuit and a chamber. The test motor and the reference heater are placed symmetrically and the heat-exchanger is situated in the middle.

4.1 Chamber

The inner dimensions of the chamber are $140 \times 120 \times 140$cm where the reference heater, test motor, and the heat-exchanger are located. In order to prevent having hot spots in the inner surface of the walls, and have homogeneous temperature, the inner surface of the walls are coated with aluminium sheets with thickness of 1 mm, since aluminium's thermal conductivity is $205\frac{\text{W}}{\text{mK}}$, which is high. The thickness of each wall is 150 mm, and the walls are made out of polyurethane. The thermal conductivity of

polyurethane is $0.023\frac{\mathrm{W}}{\mathrm{mK}}$, which is relatively low. There is a heat-leakage across the walls due to the temperature difference between the ambient and the inner surface of the walls. Heat-leakage of a wall can be expressed as :

$$P_{\mathrm{wall}} = \frac{\Delta T_{\mathrm{n}} \lambda S}{d} \tag{25}$$

where ΔT_{n} is the temperature difference across the walls, λ is the thermal conductivity of the material, S is the surface area, and d is the width of the walls respectively.

4.2 Flow Rate controller

A high Precision LCR-Series Alicat flow rate controller is used to control the water flow for the calorimeter. It can control the liquid flow rate up to $5\frac{\mathrm{L}}{\mathrm{min}}$, the maximum applied liquid pressure is up to 689 kPa, and the recommended applied liquid pressure according to its manual is 20-30 psig; therefore, a pressure regulator sets the applied water pressure to the flow rate controller[27]. For the upstream of the flow meter,

Figure 8: LCR-Series Alicat liquid flow rate controller[27]

there is a 20 micron filter, which is recommended to be maintained, and exchanged when there are sediments.

4.3 Heat-Exchanger and Fan

As discussed before, in water-cooled calorimeters, the heat-exchanger exists, and its role is to exchange the heat from air to water. The airplex GIGANT with copper fins heat-exchanger is utilized. The dimensions are 310 x 310 x 960 mm, and water pressure up to 0.8 bar is permissible. A centrifugal fan is mounted on the top of the heat-exchanger as it can be seen in Figure 9.

4.4 Test Motor

The test motor is a 37 kW fan-cooled cage induction motor with efficiency of 92%. The test motor is coupled with a 45 kW induction machine. The motor fan air flow rate is estimated 0.17 $\frac{\mathrm{m}^3}{\mathrm{s}}$. The test motor rated values are written in Table 1.

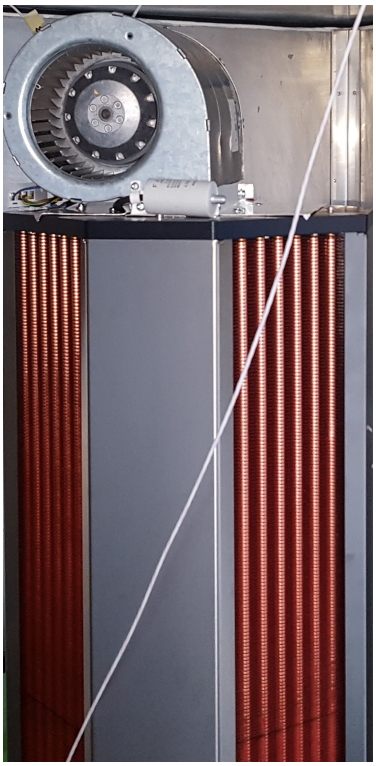

Figure 9: Heat-exchanger and the cetrifugal fan

Table 1: Rated values of the test motor

Power	Voltage	Current	Cooling	speed	Pole pair	P.F.
37 kW	380 V	72 A	TEFC	1470 rpm	2	0.84

4.4.1 Test Motor Protection

In order to fulfill the IEEE 841 Standard, the environment temperature of the test motor should not exceed 40°C[28], since insulation life drops by half for each 10 °C of overtemperature; therefore, a temperature relay is added to the set-up, a thermocouple sensor is suspended from the ceiling of the chamber on the top of the test motor to measure the air temperature with almost 20 cm distance from the test motor, and conveys the feedback to the temperature relay. There is a set-point for the temperature relay, and if the thermocouple measures temperature over 40C, the relay will be open circuit to turn off the test motor.The thermocouple is not as accurate as Pt-100 sensor; nevertheless, the thermocouple response time is shorter than Pt-100 sensor. So, it sends the feedback quicker than Pt-100 sensor.

4.4.2 Measuring Motor's Friction Loss

The test motor's friction and windage loss P_{fw} can be estimated with a separate test at no load. Initially, the test motor is supplied with the rated voltage, then the supplied voltage is reduced progressively step wise. At the corresponding voltages, the active

power and speed are recorded. Reducing the supplied voltage contributes to reduce the current, and as a result, the input power will drop. The speed remains at the rated speed at all the measured points. At some points of the measurements, when the supplied line voltage is low, ranging from 30 V to 40 V, the active power remains constant, at these points the current is too low to magnetize the core; therefore, the motor's core losses and resistive losses can be neglected. When the test motor is supplied by the low voltage, the rotational speed of the motor is still constant around 1500rpm, indicating the slip is close to zero. Figure 10 shows the non-linear fit of

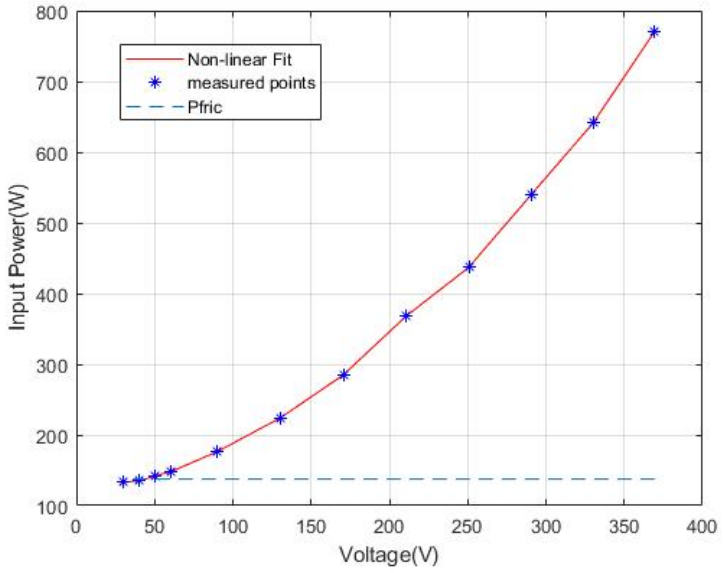

Figure 10: No-load loss as a function of voltage

the total power loss as a finction of line voltage. The star points show the measured points with the respect of the recorded powers and voltages, and the dashed blue line represents the friction and windage loss which remains constant at no load ranging from rated to very low 30V voltage.

Figure 11 shows the power loss as a function of squared voltage, the red line illustrates the linear fit of the measurement, and the initial point of the linear fit is the estimation for the friction and the windage loss at the no-load when an additional shaft and the two bearing houses are not coupled with the test motor. Therefore, the windage and the friction loss is 137 W.

4.4.3 Bearing House

Two bearing houses are required to keep the additional shaft as it is shown in figure 12. One bearing house is located inside the chamber, and the second one is fixed by an aluminium stand outside of the chamber. It is expected that the friction and winadage losses of the test motor increase due to the bearing friction losses. So, the

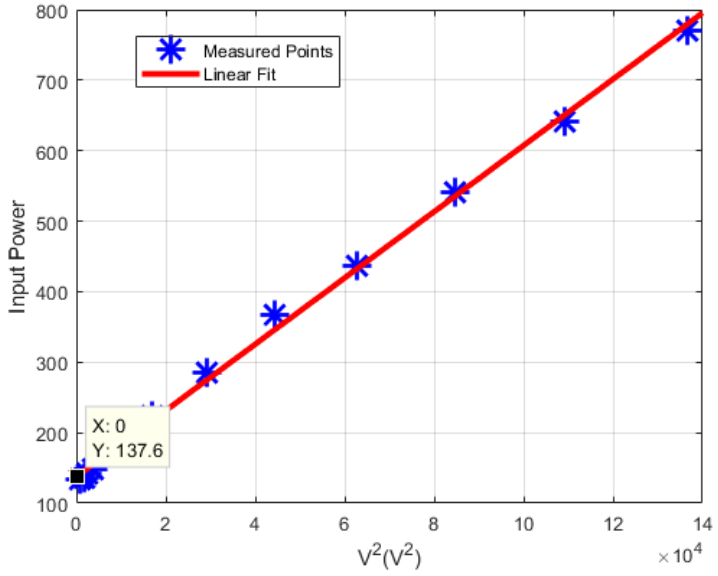

Figure 11: No-load loss as a function of squared Voltage

friction and windage losses of the test motor is measured, while the test motor is coupled with the bearing houses.

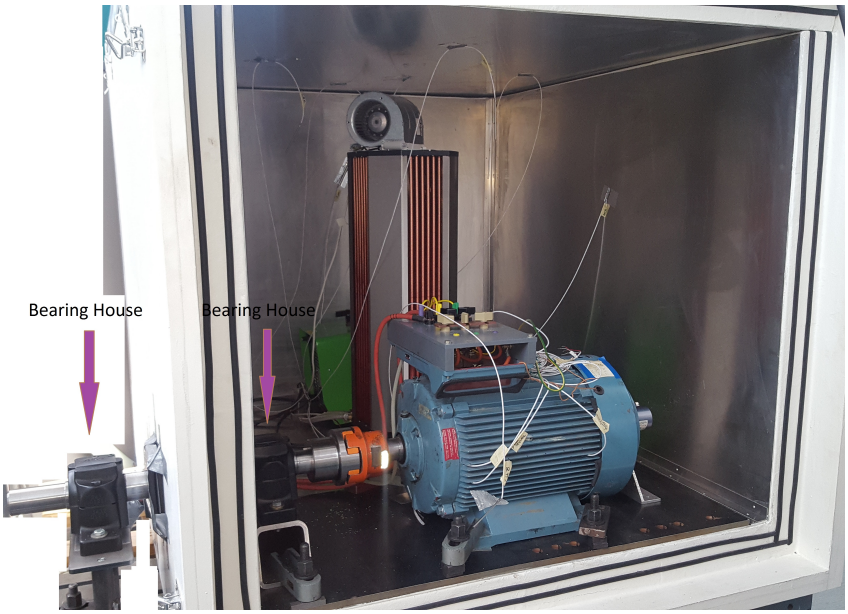

Figure 12: side view of the layout inside the chamber

Measuring the input power by a watt-meter is reliable, as the test motor is not loaded. The input power is sampled and recorded at the corresponded voltages shown in Figure 13. Comparing Figures 10 and 13 proves the friction and windage

losses are increased when the bearing houses are added to the set-up. It is estimated the friction and windage loss is 293.5 W shown in Figure 14. The difference of the friction and windage loss when the test motor is coupled and not coupled with the bearing houses is 155.9 W. The friction loss for each bearing house is roughly 77.95 W, since bearing houses are identical. These measurements must be done when the bearing houses's temperatures are stabilized.

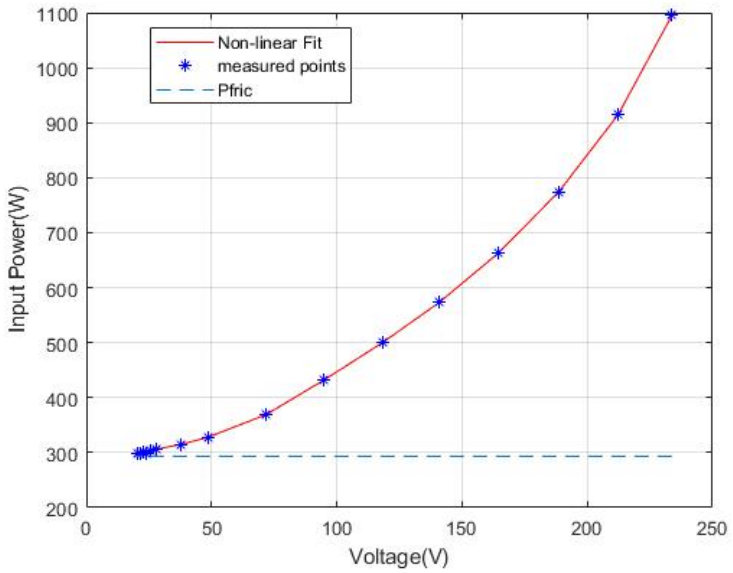

Figure 13: No-load loss as function of voltage when the additional shaft is coupled to the test motor through the bearing houses. Comparing Figures 13 and 10 shows the friction and windage losses are increased due to the additional shaft and the bearing houses.

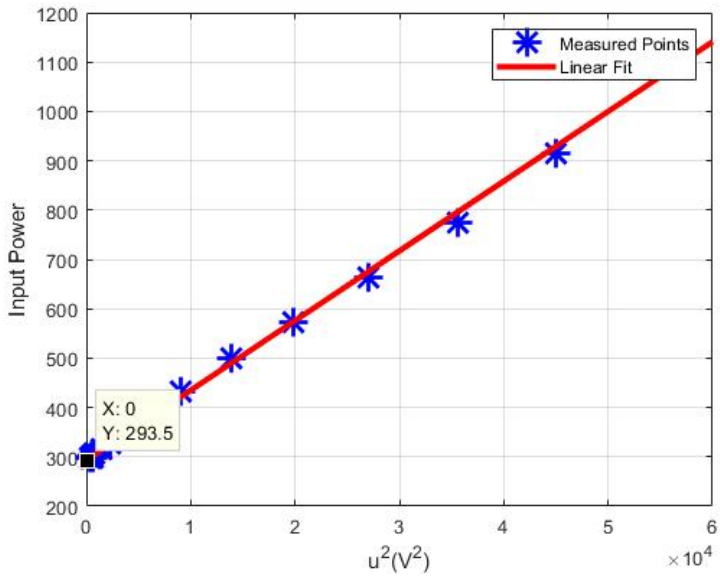

Figure 14: No-load loss as function of squared voltage when the additional shaft is coupled to the test motor through two bearing houses.

4.5 Water Circuit

The inlet water temperature must be kept constant during the long period of the calorimetric measurement, then the outlet water temperature indicates the temperature rise and the rate of thermal energy of water. Keeping the inlet water temperature constant which gets into the heat-exchanger inside the chamber is challenging, as the inlet water is supplied by the tap water with relatively high water flow rate, and the tap water temperature might vary during the calorimetric measurement. Figure 15 illustrates the inlet water circuit block diagram.

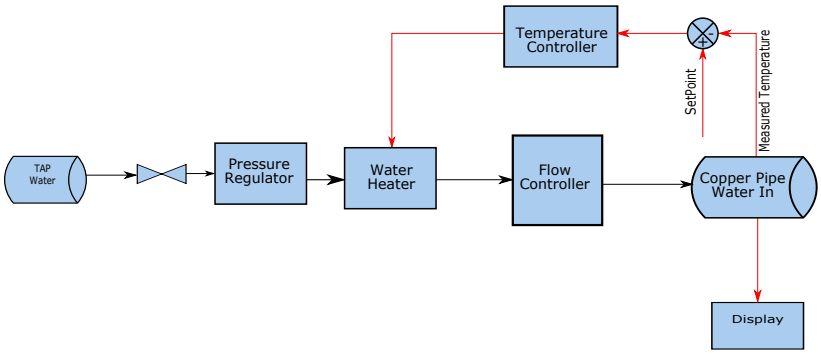

Figure 15: Block diagram of inlet water circuit

Water passes copper pipe and gets into the calorimeter. A Pt-100 sensor measures the copper pipe temperature and sends a feedback to the temperature controller. The user sets the setpoint temperature for the temperature controller, and the temperature controller adjusts the input power for the water heater in a way to obtain the desired and constant water temperature. Table 2 shows the required

Table 2: Needed power for 1°C Temperature Rise with respect to the flow rate

Flow Rate(LPM)	Required Power(W)
5	348.33
4	278.67
3	209
2	139.33

powers which are needed to be supplied by the water heater to increase the water

temperature by 1°C corresponding to the water flow rates. Assuming water density ρ is 1 $\frac{\mathrm{kg}}{\mathrm{m}^3}$ and the heat capacity of water C_p is 4.18$\frac{\mathrm{kJ}}{\mathrm{kgK}}$.

The maximum active power for the water heater, utilized in the inlet water circuit is 1140 W. The maximum water temperature rise by the 1140 W water heater at different water flow rates are listed in Table 3, assuming ρ is 1 $\frac{\mathrm{kg}}{\mathrm{m}^3}$ and C_p is 4.18 $\frac{\mathrm{kJ}}{\mathrm{kgK}}$ respectively. Table 3 shows, reducing the water flow rate contributes to increase the

Table 3: Maximum water Temperature Rise by the water heater at different water flow rates

$\dot{V}(\frac{L}{min})$	ΔT_max
5	3.27
4	4.1
3	5.45
2	8.2

water temperature rise.

Determination of setpoint temperature

The inlet water temperature setpoint must be set higher than the tap water temperature at any water flow rates to inhibit the changes in the inlet water temperature. Table 4 shows the inlet water temperatures at two conditions. The second and third columns show the water temperatures in the steady state when the water heater is off, and the water heater is operating with its maximum power respectively at different water flow rates. The difference between these two measured temperatures represents the maximum water temperature rise at different water flow rates which can be provided by the water heater.

Table 4: Maximum and minimum inlet water temperatures at different water flow rates

$\dot{V}(\frac{\mathrm{L}}{\mathrm{min}})$	$T_\mathrm{in,Min}$(°C)	$T_\mathrm{in,Max}$(°C)	$\mathrm{T_r}$
5	8.4	11.1	2.7
4	8.5	12.5	4
3	9.1	14.4	5.3
2	9.9	17.9	8

The inlet water temperature entering to the calorimeter must not be affected by the tap water temperature, which can change over seasons, months, even days and nights. In order to obtain a constant inlet water temperature, the set point temperature must be made in the range of the aforementioned conditions; meaning that the set point temperature must be greater than the measured inlet water temperature without

water heater and lower than the measured inlet water temperature when maximum power of the water heater is applied. The inlet water temperature range should be specified at different climates and seasons.

4.6 Cable Connections

The cable connections for the test motor and the reference heater in the chamber generate heat due to their resistive losses. All the elements which lead to produce heat in the chamber must be taken into account in the calculations and measurements. Resistance of a conductor can be expressed as:

$$R = \rho(L/A) \tag{26}$$

where R is the resistance of the conductor in (Ω), L is the length of the conductor in (m), A is the cross section area of the cable in mm^2, and ρ is the resistivity of the copper in ($\Omega.m$). The resistivity of the copper, the material which is used in the cables, can be changed at different temperatures. The temperature of the cables can be measured via the thermal camera, and the resistivity of conductor can be calculated based on the following equation.

$$\rho = \rho_0[1 + \alpha(T - T_0)] \tag{27}$$

where ρ is the resistivity of the conductor at temperature T, ρ_0 is the resistivity of the conductor at a reference temperature, the reference temperature T_0 is assumed 20°C, α is the temperature coefficient of the conductor, which is equal to 0.004041 for the copper at 20°C, and T is the conductor temperature, measured by the thermal camera from the joints of the cables shown in Figure 16. When the resistance of the cables are determined according to the mentioned procedure, the resistance of each cable can be multipiled by their squared current phase measured by the watt-meter.

$$P_{\text{Cable}} = RI_{\text{ph}}^2 \tag{28}$$

where, P_{Cable} is the power loss of the cable, I_{ph} is the phase current.

4.7 Reference Heater

The rated power and voltage are 6 kW and 400 V respectively for the three phase Remko Elkomat electric heater, which is used as a reference heater. The reference heater entails a temperature relay, and it will be open circuit if the ambient temperature exceeds the certain set-point value, which is set by a user. In addition, the reference heater has its own fan. Whether the heater heats up or not, the heater's fan can run, and can operate individually. Air flow rate for the heater's fan is $0.14\frac{\text{m}^3}{\text{s}}$. An auto-transformer controls the input voltage, and Fluke NORMA 5000 measures the power loss of the reference heater.

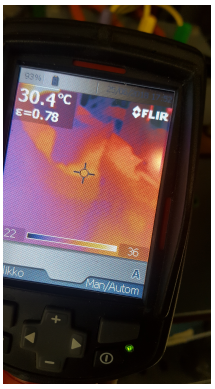

Figure 16: Measuring the joint temperature of the test motor's cable via thermal camera

4.8 Insulation

There are three holes on the walls of the calorimeter . A hole is dedicated for the balance heater cable connections, inlet and outlet water pipes, the Pt-100 sensors, ventilation and a protection relay cable connections for the balance heater. In order to reduce the hole heat-leakage, the hole is insulated as shown in Figure 17. The hole

Figure 17: Hole Insulation

is insulated by three Armaflex gasket layers, and the air gaps between the cables are insulated by the Armaflex pieces. Furthermore, there are two holes for the test motor cable connections and the shaft. Figure 18 shows the inner view of the wall of the calorimeter which there are two holes for the shaft and test motor cable connections. Figures 19 and 20 show the insulation for the cable connection of the test motor and shaft respectively. Like the previous hole, the holes are insulated with three Armaflex layers, and the gaps are filled with Armaflex pieces for the motor cable connections hole. In order to prevent the shaft heat-leakage during the balance tests, which basically happens due to the convection from the shaft hole and conduction due to the conductivity of the shaft, a Finnfoam chamber covers the bearing house, the

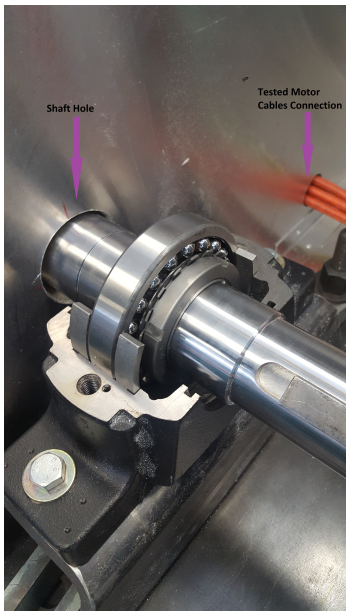

Figure 18: Holes for shaft and test motor cable connections inner view

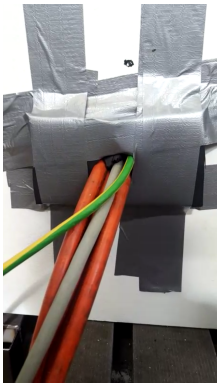

Figure 19: Insulation test motor cable connection

shaft, shaft hole and test motor connection hole. Figure 21 shows how the Finnfoam chamber covers the shaft, the shaft hole and the test motor cable connections when the test motor is not coupled with the loading machine. During the balance test, the Finnfoam chamber covers two holes. Nevertheless, during the actual test, the test motor is coupled with the loading machine. Figure 22 shows the insulation of the shaft during the actual tests, and when the test motor is coupled with the loading machine. A Finnfoam chamber covers the bearing house where the shaft passes, the gaps are covered with Armaflex pieces.

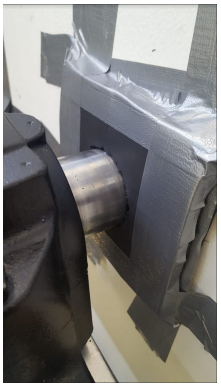

Figure 20: Thermal insulation for the shaft hole with three Armaflex layers

Figure 21: Finnfoam chamber

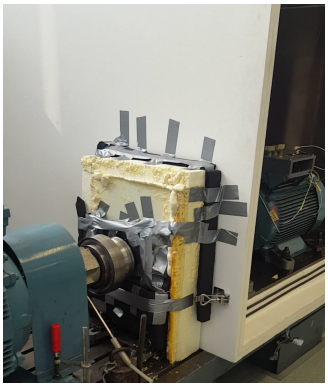

Figure 22: Shaft insulation when the test motor is coupled with the loading machine

5 Assessment During Assembling Process

5.1 Calorimetric Tests with Reference Heater

It is highly recommended to observe and justify the behaviour of the calorimeter, before putting the test motor inside the chamber, and before making the holes for the shaft and cable connections of the induction test motor, as the air temperature inside the chamber might not be suitable for the test motor, and having more holes on the walls lead to increase the heat-leakage. Figure 23 shows a side view of the calorimeter, when there are balance heater and the heat-exchanger in the chamber, while there are no test induction motor, shaft hole and cable connections hole for the induction test motor. During the tests, total loss in the chamber entails the reference

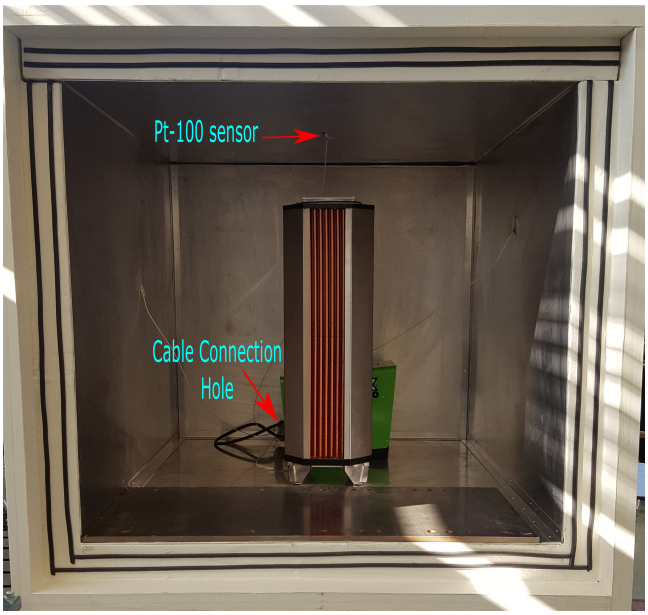

Figure 23: Side view of the calorimeter with only one hole for the cable connections

heater loss, it's fan loss, and the heat exchanger's ventilation loss. The reference heater's fan has its own cable connection and it runs in all the tests. The total loss during the tests can be expressed as:

$$P_{\text{total}} = P_{\text{fan,hex}} + P_{\text{fan,res}} + P_{\text{res}} \tag{29}$$

$$P_{\text{vent}} = P_{\text{fan,hex}} + P_{\text{fan,res}} \tag{30}$$

$$P_{\text{total}} = P_{\text{vent}} + P_{\text{res}} \tag{31}$$

where $P_{\text{fan,hex}}$ is the loss for the heat-exchanger's fan, $P_{\text{fan,res}}$ is the loss for the reference heater's fan and P_{res} is the reference heater loss. The reference heater's fan and the heat-exchanger's fan power losses can be accumulated and represents the ventilation power loss P_{vent} .

Table 5: Test results

P_{res}(W)	$P_{\text{fan,res}}$(W)	$P_{\text{fan,hex}}$(W)	P_{total}(W)	P_{W}(W)	$\overline{\theta_{\text{Cham}}}$(°C)	θ_{amb}(°C)
1000	33.2	9.05	1042.25	1042.56	24.82	22.64
2000	33.2	9.05	2042.25	2012.52	41.18	21.65
3000	33.2	9.05	3042.25	2936.76	56.68	22.72
4000	33.2	161.5	4194.7	4148.97	36.06	24.07

Figure 24: Six DC fans used as the heat-exchanger ventilation

Table 5 shows the measured thermal energy of water P_{W}, ambient temperature θ_{amb},the total loss, power loss components, and the average air temperature $\overline{\theta_{\text{Cham}}}$ in the chamber. All the tests are executed with $5\frac{\text{L}}{\text{min}}$ constant water flow rate and 9.5°C constant inlet water temperature. The total loss and the loss components are measured through the power analyser. The loss components are constant, so power analyser is accurate and reliable; therefore, if the water thermal energy is near to the measured total loss via the the power analyser, the calorimeter results are accurate as well.

Initially six DC fans have been mounted to one of the inner walls of the heat-exchanger as shown in figure 24. The tests with 1 kW, 2 kW and 3 kW of reference heater loss are done with the six DC fans. In the test with 3 kW of the reference heater loss, the average air temperature inside the chamber is almost 56°C, which is quite high ambient temperature for the test motor. The average air temperature is determined by four Pt-100 temperature sensors which are suspended in the chamber with 20 cm off to each wall and the ceiling inside the chamber. In order to combat this high air temperature, instead of six DC fans as the ventilation for the heat-exchanger, a 161.5 W centrifugal fan shown in Figure 9 is mounted on the top of the heat-exchanger. The test with 4 kW reference heater loss is done when the centrifugal fan used as the heat-exhanger's fan. It is observed when the total loss is almost 4 kW, the calorimeter average air temperature is 36°C which fulfills the ambient temperature restrictions for motors.

The 37 kW test motor is 92% efficient, and it is expected at full-load the upper limit for the total loss in the chamber is 4 kW. Hence, the calorimeter equipped with the centrifugal fan can keep the air temperature below 40 °C for the test motor.

5.2 No-load Tests Without Additional Shaft

These tests are made with the test motor at no-load, when the motor is not coupled with the additional shaft, and there is no shaft hole on the wall. The loss of the induction motor at no-load can be measured reliably by the power analyser, since the motor isn't loaded with the loading machine, and the slip is almost zero. Comparing the measured water thermal energy and power analyser results indicates how the calorimeter is accurate. Table 6 shows the calorimetric measurements at no-load at different water flow rates.

Table 6: No-load tests results without additional shaft

P_{loss}(W)	P_{vent}(W)	P_{total}(W)	P_{W}(W)	$\dot{V}(\frac{\text{L}}{\text{min}})$	θ_{Cham}(°C)	θ_{amb}(°C)
922.8	197	1119.8	1102.33	2	27.73	23.97
919	197	1116	1138.62	3	22.51	24.95
923.2	197	1120	1212.04	5	17.53	24.02

The results show how the water flow rate affects the chamber's temperature. Increasing the water flow rate brings about lowering the chamber's temperature. The measured coolant power P_{W}(W) with 3 and 5 $\frac{\text{L}}{\text{min}}$ are higher than the measured power through the power analyser, as the chamber's temperatures in these experiments are lower than the ambient temperature; therefore, there is a heat-leakage from ambient to the chamber. Nevertheless, in the test with 2 $\frac{\text{L}}{\text{min}}$ the chamber's temperature is higher than the ambient temperature, so the heat-leakage flow direction is from chamber to ambient, and the measured thermal energy of water is lower than the measured power through the analyser. The thermal energy of water at no-load with 2 $\frac{\text{L}}{\text{min}}$ water flow rate is 98.4 % accurate if the power analyser measurement is considered as the reference.

5.3 No-load Tests With Additional Shaft

Unlike the previous tests, these tests are done at no-load when the induction motor is coupled with the additional shaft, and there is a shaft hole on the wall, and the shaft passes through the shaft hole. Nevertheless, the shaft is not coupled with the loading machine. The following table shows the no-load test measurement results at 2 and 5 $\frac{\text{L}}{\text{min}}$.

Table 7: No-load tests results with the additional shaft

P_{loss}(W)	P_{vent}(W)	P_{total}(W)	P_{W}(W)	$\dot{V}(\frac{\text{L}}{\text{min}})$	$\overline{\theta_{\text{Cham}}}$(°C)	θ_{amb}(°C)
1062.8	197	1259.8	1201.7	2	28.95	24.18
1138.5	197	1335.5	1344	5	18.4748	26.25

If the power analyser loss measurements are assumed as reference, the inaccuracy of the measured thermal energy of water in the previous test is 1.6 %, When the water flow rate is 2 $\frac{\text{L}}{\text{min}}$. While, when the water flow rate is 2 $\frac{\text{L}}{\text{min}}$, and the additional shaft is coupled with the test motor and passes through the shaft hole, the inaccuracy

of the measured thermal energy of water is 4.6 %. The inaccuracy of the calorimeter at no-load when the water flow rate is set at 2 $\frac{\mathrm{L}}{\mathrm{min}}$ is increased by 3 % , when the shaft hole and the additional shaft are added to the calorimeter. It can be deduced, the most heat-leakage occurs due to the shaft heat-leakage at no-load when the water flow rate is 2 $\frac{\mathrm{L}}{\mathrm{min}}$.

6 Measurement

6.1 Actual Test

During the actual test or test run, the calorimetric measurements are conducted with the test motor. The power loss of the test motor includes friction and windage losses, stator and rotor resistive losses, and core losses. The last three losses are regarded as the electromagnetic losses. The test motor loss can be expressed as:

$$P_{\text{loss}} = P_{\text{fw}} + P_{\text{s}} + P_{\text{r}} + P_{\text{fe}} = P_{\text{fw}} + P_{\text{em}} \tag{32}$$

The total loss during the test run can be expressed as:

$$P_{\text{total}} = P_{\text{fw}} + P_{\text{em}} + P_{\text{vent}} + P_{\text{Cable}} \tag{33}$$

During the actual test the fan of the balance heater runs to generate homogeneous heat flow in the chamber. The ventilation loss P_{vent} includes the losses for the heat-exchanger and the reference heater fans. Also, there are losses due to the cable connections.

The rate of thermal energy of water during the actual test can be expressed as:

$$\Delta Q_{\text{t}} = P_{\text{total}} \pm q_{\text{t}} \tag{34}$$

The plus and minus sign for the heat-leakage indicates the heat-leakage flow direction. When the chamber's temperature is lower than the ambient temperature, the heat-leakage flow is from ambient to the chamber; therefore, the coolant power ΔQ_{t} would be greater than the total loss in the chamber. Nevertheless, if the chamber's temperature is higher than the ambient temperature, the heat-leakage flow direction is from the chamber to the ambient. In the latter case, the rate of thermal energy of water is less than total loss P_{total}. When the chamber's temperature is higher than the ambient temperature, the rate of thermal energy is expressed as:

$$\Delta Q_{\text{t}} = P_{\text{total}} - q_{\text{t}} \tag{35}$$

It is observed when the total loss is less than 2.5 kW in the chamber, and the water flow rate is $5\frac{\text{L}}{\text{min}}$, the chamber's temperature is lower than the ambient temperature. For the total losses less than 2.5 kW, the calorimetric tests are done with $2\frac{\text{L}}{\text{min}}$ water flow rate, and above 2.5 kW total losses, the water flow rate is set at $5\frac{\text{L}}{\text{min}}$. So, in all tests, the chamber's temperature is higher than the ambient temperature and the heat-leakage flow direction is known.

6.2 Balance Test

The balance test is conducted with the balance heater to reach the same temperature rise for the coolant as the actual test, with the same water flow rate. During the balance test, the main heat source is the 6 kW balance heater. In order to pursue

the same heat flow in the chamber during the balance tests and the actual tests, the balance heater's fan and the test motor's fan run simultaneously. The test motor's fan runs while the test motor is not loaded, and it rotates with its rated speed at low voltage.

During the balance test, there are five heat sources inside the chamber. The first and the main one is the balance heater loss P_{res}. The balance heater's loss is controlled via an auto-transformer. The second one is the heat-exchanger's fan loss $P_{\text{fan,hex}}$. The third one is the balance heater's fan loss $P_{\text{fan,res}}$. The forth is the friction and windage loss of the test motorP_{fw} including the bearing's friction loss. The test motor magnetic loss in this case is negligible. The fifth loss component is the loss due to the cable connections. The friction loss for the bearing house outside of the chamber must be subtracted from the measured loss of the test motor, as the loss components in the chamber are considered in the measurements and calculations. The total loss during the balance test is expressed as:

$$P_{\text{total}} = P_{\text{res}} + P_{\text{fw}} + P_{\text{vent}} + P_{\text{Cable}} \tag{36}$$

The thermal energy of water during the balance test is expressed as:

$$\Delta Q_{\text{b}} = P_{\text{res}} + P_{\text{fw}} + P_{\text{vent}} + P_{\text{Cable}} \pm q_{\text{b-walls}} \pm q_{\text{b-holes}} \pm q_{\text{b-shaft}} \tag{37}$$

where ΔQ_{b} represents the rate of thermal energy of water, and $q_{\text{b-walls}}$, $q_{b-holes}$, $q_{b-shaft}$ are the heat-leakages for walls, holes and shaft respectively. Rate of thermal energy of water can also be expressed as:

$$\Delta Q_{\text{b}} = P_{\text{total}} \pm q_b \tag{38}$$

Where q_{b} is the total heat-leakage during the balance test. Balance tests are made when the chamber's temperature is higher than the ambient temperature, so the rate of thermal energy of water can be expressed as:

$$\Delta Q_{\text{b}} = P_{\text{total}} - q_{\text{b}} \tag{39}$$

When the rate of thermal energy and the heat-leakage during the balance test are equal to the rate of thermal energy and the heat-leakage during the actual test, the balance heater loss during the balance test is equal to the electromagnetic loss of the test motor during the actual test.

6.3 Time Constant

Electrical engineers find it helpful to visualize the thermal model as an electrical analog circuit. The first order equation of the thermal model has the same form as the equation expressing the voltage rise in an electrical RC circuit[29]. The thermal resistance and capacitance of the balance heater and the test motor are analogous to the electrical resistance and capacitance. Response to the loss step can be solved from the differential equation[30]:

$$\Theta(t) = \Theta_0 + (\Theta_\infty - \Theta_0)(1 - e^{-t/\tau_{\text{th}}}) \tag{40}$$

where Θ_0 is the the temperature at initial time of the test, Θ_∞ is the temperature at infinite, and τ_{th} is the thermal time constant. During the balance test, the main heat source in the chamber is the balance heater, so the time constant of the calorimeter at balance test is oriented by the time constant of the balance heater.

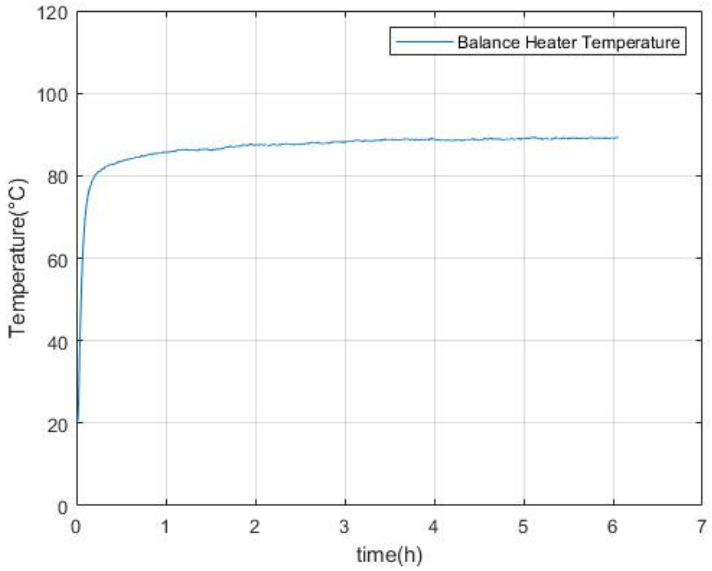

Figure 25: Balance heater temperature rise

Figure 25 shows a Pt-100 sensor temperature measurements which is attached to the steel protection frame of the balance heater to measure the temperature rise, when the balance heater loss is 3kW. It takes almost 6 hours for the balance heater to reach the steady state based on the calorimetric standards. The balance heater temperature reaches steady state when its temperature does not vary more than ± 0.3[31]. The time required to reach 63 percent of the the infinite or steady state temperature describes the time constant:

$$\Theta(\tau_{\text{th}}) \cong 0.63\Theta(\infty) \tag{41}$$

where $\Theta(\tau_{\text{th}})$ is the temperature at time constant, $\Theta(\infty)$ is the temperature in the steady state or infinite. The time constant of the balance heater is about 40 min, when its power is set at 3 kW.

The thermal time constant during the actual test is governed by the test induction motor. There is evidence that relatively simple models can represent major phenomena associated with thermal behavior of electric motors and drives[32]. Thermal limit curves of induction motors are widely adopted in industry, and define safe operating times for various levels of input currents, are fundamentally equivalent to thermal protection based on the first-order thermal model[33]. Figure 26 shows the temperature measurements of the drive end-end windings. The thermal time constant for the test induction motor is almost 60 minutes when the motor is at

no-load. The end winding's temperature reaches to steady state in 8 hours. So, the thermal time constant of the calorimeter is 8 hours.

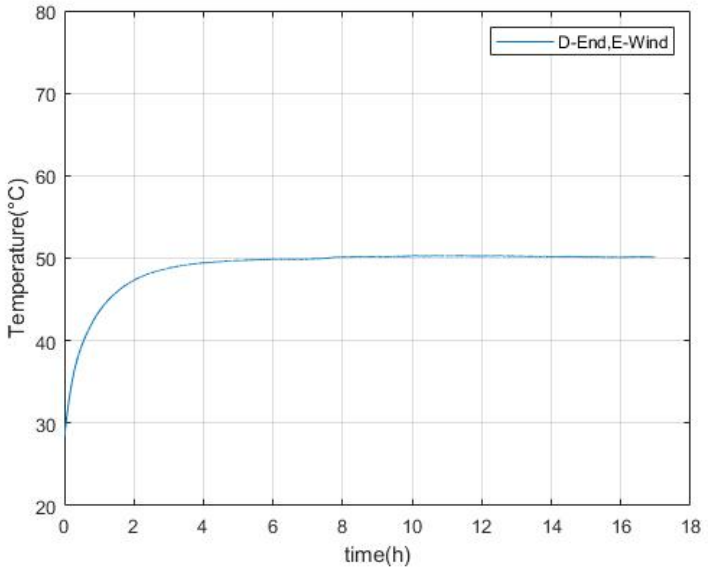

Figure 26: Drive end-end winding temperature rise at no-load

6.4 Calibration Curves

Having a calibrated calorimeter prevents doing the balance test after each actual test, and reduce the balanced calorimetery process time by half[34] . A calibration curve can be obtained by several calorimetric tests conducted by the balance heater at different power levels. The thermal energy of water is measured and sampled at different power levels of the balance heater in the steady state.

It is observed when the total loss in the chamber is lower than 2.5 kW, and the water flow rate is $5\frac{\mathrm{L}}{\mathrm{min}}$, the chamber's temperature is lower than the ambient temperature. While, with 2 $\frac{\mathrm{L}}{\mathrm{min}}$ water flow rate, the chamber's temperature is higher than the ambient temperature for the range of total loss below 2.5 kW. In addition, in order to keep the chamber's temperature lower than 40° C, the water flow rate must be set at $5\frac{\mathrm{L}}{\mathrm{min}}$ for the total losses higher than 2.5 kW in the chamber. Two calibration curves with 2 and 5 $\frac{\mathrm{L}}{\mathrm{min}}$ for total losses less than 2.5 kW and higher than 2.5 kW are employed respectively. Then, all the tests have the same heat-leakage flow direction. Figure 27 shows the calibration curve with 5 $\frac{\mathrm{L}}{\mathrm{min}}$, and the deviation of the measured samples from the fitting line of the calibration curve. The calibration curve can be expressed as:

$$\Delta Q_{\mathrm{b}} = 0.9545 P_{\mathrm{res}} + 480\mathrm{W} \tag{42}$$

Equation 42 indicates water absorbs 95% and miss 5% of the total loss. Figure 28

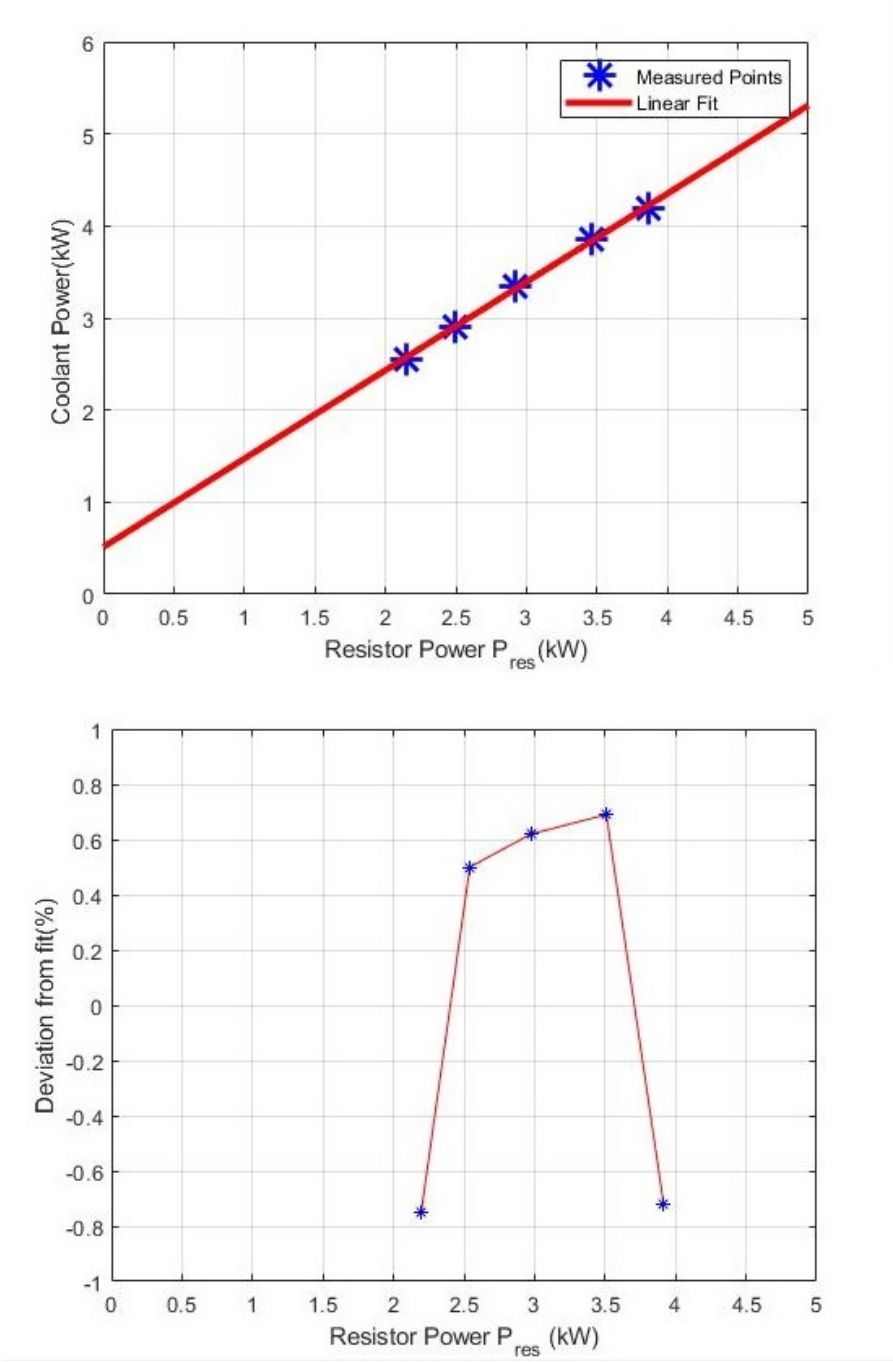

Figure 27: Calibration curve with 5 $\frac{\mathrm{L}}{\mathrm{min}}$

shows the calibration with 2 $\frac{\mathrm{L}}{\mathrm{min}}$ water flow rate and deviation of the measured point from the calibration curve's fitting line. The calibration curve with 2 $\frac{\mathrm{L}}{\mathrm{min}}$ is expressed as:

$$\Delta Q_{\mathrm{b}} = 0.956 P_{\mathrm{res}} + 422\mathrm{W} \tag{43}$$

The difference between the total loss and the rate of thermal energy of water

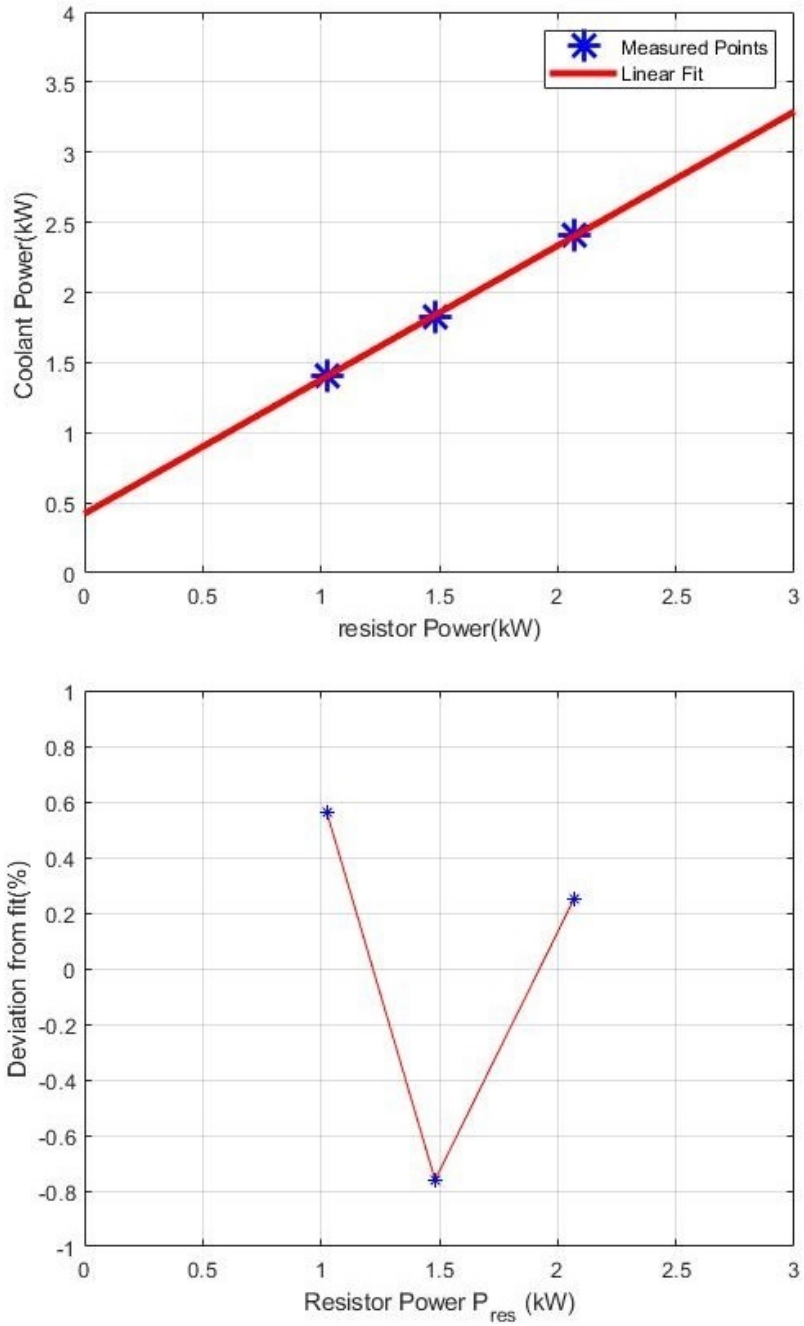

Figure 28: Calibration curve with 2 $\frac{\mathrm{L}}{\mathrm{min}}$

is due to the heat-leakage. Unlike the actual test, during the balance tests, the loss components are measured reliably with the power analysers. Nevertheless, the friction and windage losses of the test motor and the friction loss of the bearing house are based on the estimation. The heat-leakage is estimated for the calibration curve with 5 $\frac{\mathrm{L}}{\mathrm{min}}$ water flow rate. Figure 29 shows the heat-leakage is about 100 W,

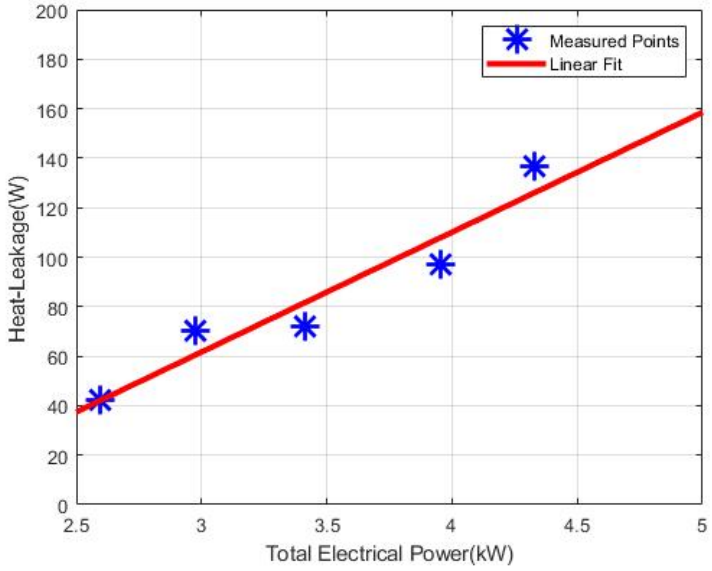

Figure 29: Heat-leakage at 5 $\frac{\text{L}}{\text{min}}$

when the total loss in the chamber is 4 kW. Figure 30 shows the heat-leakage during

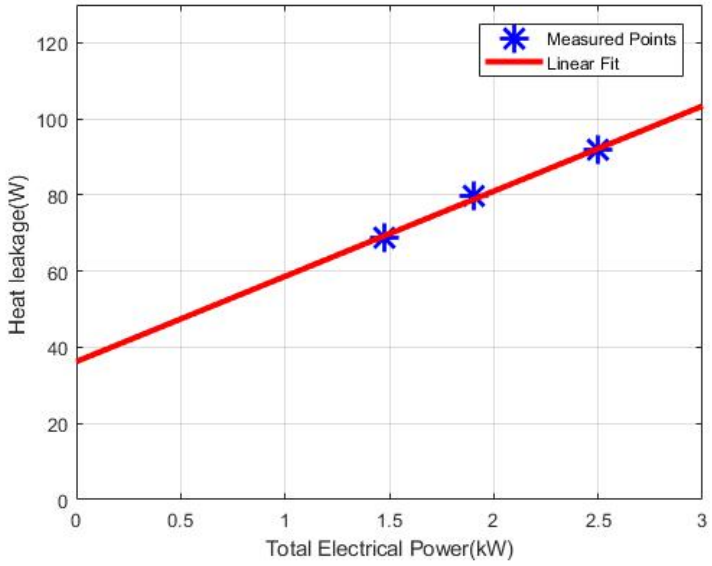

Figure 30: Heat-leakage at 2 $\frac{\text{L}}{\text{min}}$

the balance test when the water flow rate is 2 $\frac{\text{L}}{\text{min}}$. The heat-leakage is almost 90 W when the total loss in the chamber is 2.5 kW. It is expected the actual tests and the balance tests have almost the same heat-leakages.

There is a Pt-100 temperature sensor 20 cm off from the wall and 20 cm off

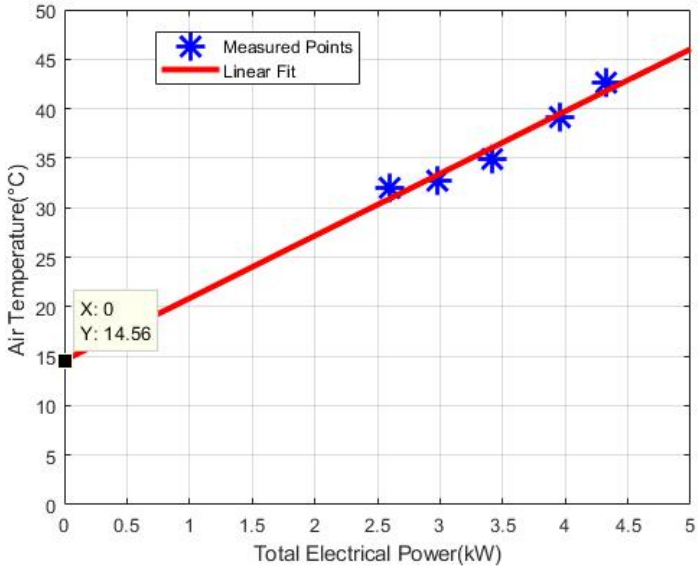

Figure 31: Air temperature at the near point to the balance heater at 5 $\frac{\text{L}}{\text{min}}$

from the ceiling where the reference heater is located. During the balance tests, the temperature sensor measures the air temperature near to the reference heater as shown in Figure 31. The air temperature is less than 40° C when the total loss is 4 kW while the water flow rate is 5 $\frac{\text{L}}{\text{min}}$. It is expected the air temperature at the near point to the test motor during the actual tests are similar to those during the balance tests. The linear relationship of the air temperature and the total loss during the balance tests is expressed as:

$$T_{\text{air}} = 6.3P_{\text{total}} + 14.56°\text{C} \tag{44}$$

6.5 Results

The coolant reaches to thermal equilibrium or the thermal steady state condition when the coolant power does not vary more than ±1% over a period of two hours or the coolant temperature rise is constant within ±1% in one hour, while the mass flow rate is constant. Moreover, the inlet coolant temperature or the winding temperature of the test motor does not vary more than ±0.3°C [31].

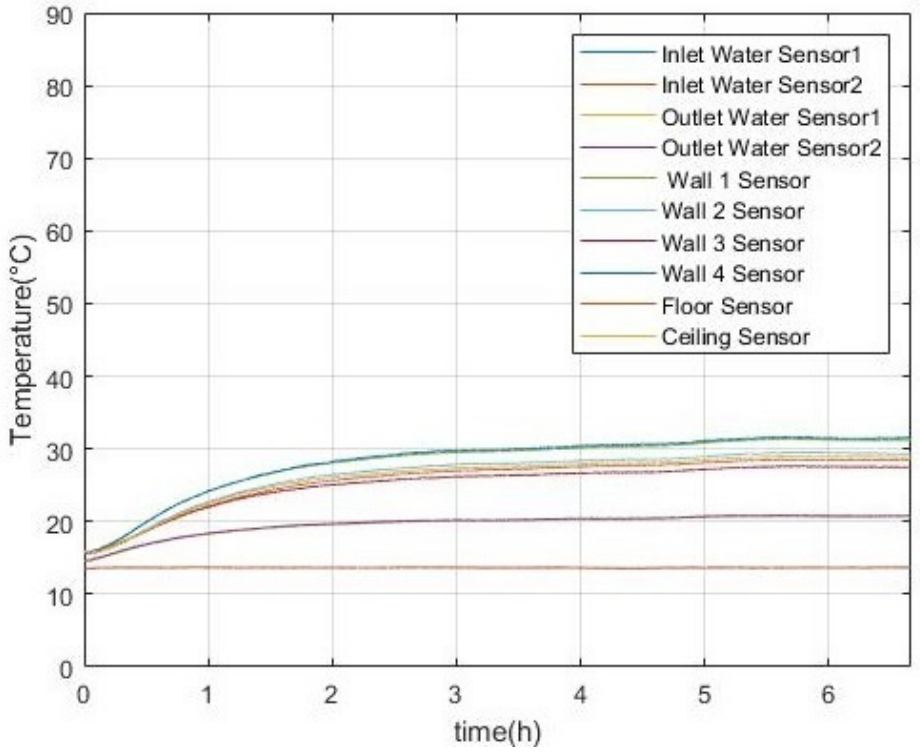

Figure 32: Temperature measurement data

Figure 32 shows the measured temperatures when the load torque is 201 Nm, and the water flow rate is 5 $\frac{\text{L}}{\text{min}}$. Two sensors measure the inlet temperature, two sensor measure outlet temperature, six sensors measure the walls, floor and ceiling temperatures.

Figure 33 shows the temperature measurements at six points of the test motor measured by six Pt-100 sensors. Drive end-end windings temperature has the highest temperature among other points. These temperature measurements are done when the load torque is 201 Nm. Figure 34 shows the ambient and air chamber's temperature measurements when the load torque is 201 Nm. The temperature measurements successfully fulfill the calorimeteric measurement criteria.

6.5.1 Heat Compensation Method

During the balance tests, the test motor is not loaded with the loading machine, and a Finnfoam chamber covers all the shaft to prevent the shaft heat-leakage due to

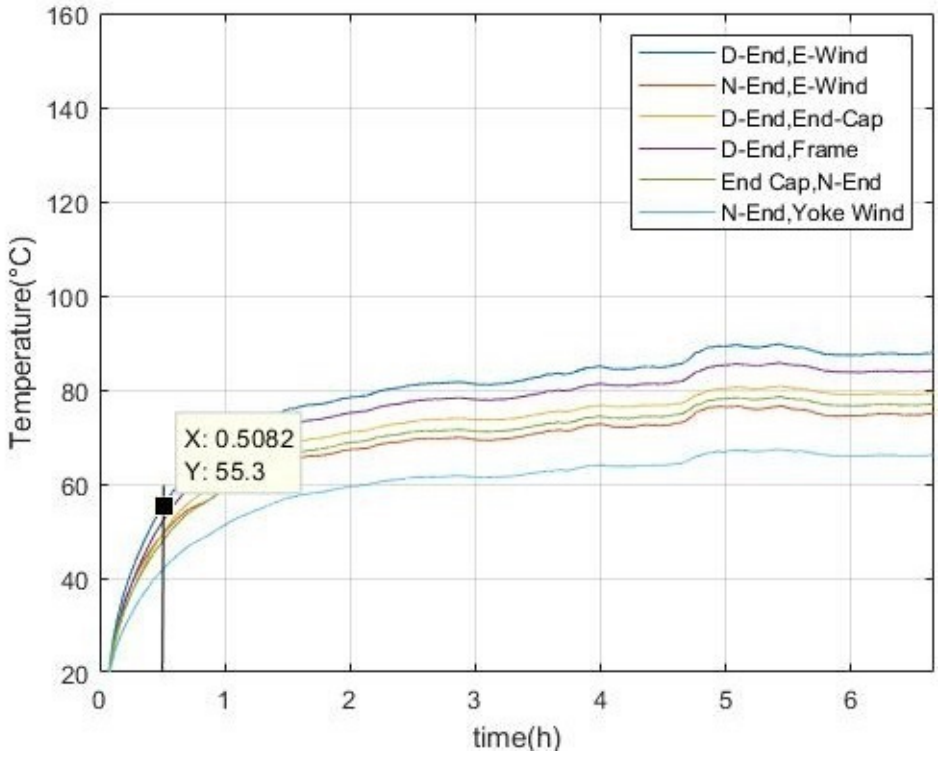

Figure 33: Temperature measurement of the test motor

the convection and the conduction. However, during the actual tests, the test motor is loaded with the loading machine. The shaft insulation covers the bearing house outside of the chamber, and prevents the shaft heat-leakage due to only convection. The shaft temperature is measured at two points shown in Figure 35. The first point is where the shaft is passing the wall inside the chamber, and the second point is where the shaft is passed from the wall outside of the chamber. In order for accurate shaft temperature measurement via a thermal camera, the steel shaft is sprayed with black color at the points.

The distance between two points is 245 mm, the radius of the shaft is 30 mm, and the thermal conductivity of the steel shaft is 54 $\frac{\mathrm{W}}{\mathrm{mK}}$[35]. The heat-leakage due to the conduction can be approximated as:

$$\frac{Q}{\Delta t} = -KA\frac{\Delta T}{d} \tag{45}$$

where $\frac{Q}{\Delta t}$ is the rate of heat flow in W, K is the thermal conductivity of the material in $\frac{\mathrm{W}}{\mathrm{mK}}$, A is the surface area of the additional shaft in m^2, d is the distance between the mentioned points, and ΔT is temperature difference between two points in K.

After each actual test, the temperature at these two points are measured, and the heat-leakage due to the conduction are calculated and considered in calibration curves. Considering the heat-leakage due to the conduction, makes the calibration

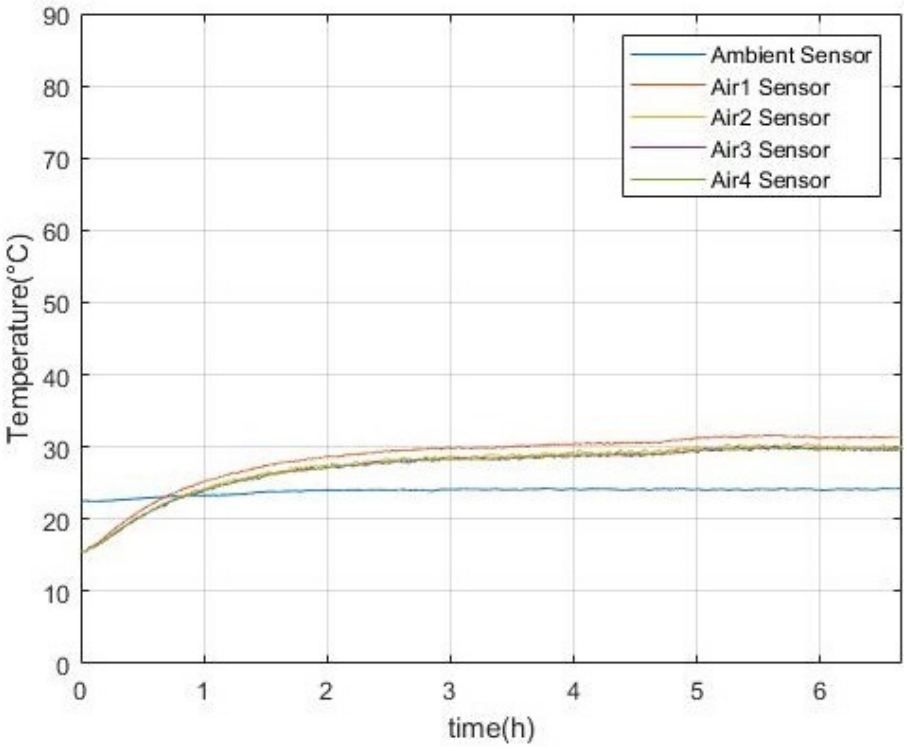

Figure 34: Air chamber and ambient temperature measurements

curve equation for 5 $\frac{\text{L}}{\text{min}}$ in a new form as :

$$\Delta Q_{\text{b}} + q_{\text{cond}} = 0.9545 P_{\text{res}} + 480\text{W} \tag{46}$$

where q_{cond} is the shaft heat-leakage due to the conduction at 5 $\frac{\text{L}}{\text{min}}$. Also, the calibration equation for 2 $\frac{\text{L}}{\text{min}}$ is rewritten as :

$$\Delta Q_{\text{b}} + q'_{\text{cond}} = 0.956 P_{\text{res}} + 422\text{W} \tag{47}$$

where q'_{cond} is the shaft heat-leakage due to the conduction at 2 $\frac{\text{L}}{\text{min}}$. After each actual test, the shaft temperatures at two points are measured in order to estimate the heat-leakage due to the conduction. The shaft heat-leakage due the conduction is 12 W when the water flow rate is 2 $\frac{\text{L}}{\text{min}}$ and the load torque is 103 Nm. When the water flow rate set at 5 $\frac{\text{L}}{\text{min}}$, and the load torque is 201 Nm, the shaft heat-leakage is 7.7 W. In table 8, $T_1(^\circ\text{C})$ and $T_2(^\circ\text{C})$ are the measured shaft temperature at the points where the shaft is passing the wall in the chamber, and the shaft after passing the shaft insulation outside of the calorimeter respectively.

6.5.2 Electromagnetic Loss

Table 9 shows the electromagnetic loss of the 37 kW induction motor at different loads, measured through calorimetric and input-output methods. The actual tests at no-load and at 103 Nm torque are done with 2 $\frac{\text{L}}{\text{min}}$ water flow rate, as the estimated

Figure 35: Using thermal camera to measure shaft temperature

Table 8: Compensated heat-leakage due to conduction

$\dot{V}(\frac{\mathrm{L}}{\mathrm{min}})$	M(Nm)	T_1(°C)	T_2(°C)	q_{cond}(W)
2	103	57.4	45	12
5	201	54	38.1	7.7

total loss in the chamber is less than 2.5 kW. The test at 201 Nm load is done with 5 $\frac{\mathrm{L}}{\mathrm{min}}$ water flow rate, since the total loss in the chamber is higher than 2.5 kW. Furthermore, third column shows the rate of thermal energy of water during the actual tests.

Table 9: Electromagnetic loss of the 37 kW induction motor measured by the calorimetric and input-output methods

M(Nm)	$\dot{V}(\frac{\mathrm{L}}{\mathrm{min}})$	ΔQ_{t}(kW)	P_{em}(kW)Calorimetry	P_{em}(kW)input $-$ output
No-load	2	1.2020	0.816	0.77
103	2	1.5592	1.202	1.246
201	5	2.6433	2.274	2.23

7 Conclusion and Future Work

7.1 Conclusion

The balanced water-cooled calorimeter is designed, constructed and calibrated for the 37 kW induction motor. Calorimetric measurements are made for the test induction motor, and the electromagnetic power loss of the induction motor is measured at different loads and no-load in both calorimetry and input-output methods. It is observed at no-load tests, the shaft hole is the place where the highest heat-leakage happens. The IEC 34-2 calorimetric standards are studied, and the calorimetric measurements met the IEC 34-2 standards.

The thermal time constant of the calorimeter during the actual test at no-load is almost 8 hours. The test motor has the highest thermal mass in the chamber, so the thermal time constant of the calorimeter can be determined by the thermal time constant of the test motor. The required time to reach 63% of the steady state end windings temperature indicates the thermal time constant of the test motor.

If the rate of thermal energy of water and the heat-leakage during the actual test are equivalent to those at the balance test, the balance heater loss during the balance test is equal to the electromagnetic loss of the test motor during the actual test. However, the heat-leakage during the actual test and the balance test are not equal due to having the different placement, the different surface areas and the different heat distributions of the test motor and the balance heater. Heat compensation method is suggested to mitigate the heat-leakage difference during the actual and the balance tests. During the balance tests, the shaft hole is entirely insulated by the Finnfoam chamber to prevent the heat-leakage due to the convection of the shaft hole and the conduction of the steel shaft. During the actual test, the Finnfoam chamber covers the bearing house outside of the chamber and prevents the heat-leakage due to the convection of the shaft hole. The heat-leakage due to the conduction of the shaft can be estimated at each actual test by measuring the shaft temperatures at points where the shaft passes the wall inside the chamber and the shaft passes the insulation outside of the chamber. So, the calibration curve equations, make new forms when the heat-leakage due to the conduction is added to the measured rate of thermal energy of water.

7.2 Future Work

A closed-cycle water-loop is suggested for the water circuit with a water pump, and a water tank. Firstly, the inlet water temperature is not affacted by the tap water. Secondly, a closed water loop reduces the water consumption. If a calorimetric test takes 7 hours and the water flow rate is $5\frac{\mathrm{L}}{\mathrm{min}}$, almost 2100 L of water is required for each calorimetric test.

In addition, the mechanical bearing houses and couplings could be replaced with the electromagnetic coupling, since the mechanical bearings and coupling power loss are not constant, and vary by the load torque and temperature [36] [37].

References

[1] Aarniovuori, L., Kolehmainen, J., Kosonen, A., Niemelä, M., Chen, H., Cao, W. and Pyrhönen, J., 2016. Application of calorimetric method for loss measurement of a SynRM drive system. *IEEE Transactions on Industrial Electronics, 63(4)*, pp.2005-2015.

[2] Waide, P. and Brunner, C.U., 2011. Energy-efficiency policy opportunities for electric motor-driven systems.

[3] Rotating electrical machines- Part 2: Methods for determining losses and efficiency of rotating electrical machinery from test(excluding machines for traction vehicles) . IEC 34-2, 1972.

[4] Daut, I., Anayet, K., Gomesh, N., Asri, M. and Muzhar, M., 2010, June. Core loss measurements of three phase AC induction motor. In *Power Engineering and Optimization Conference (PEOCO), 2010 4th International* (pp. 78-81). IEEE.

[5] Jalilian, A., 1997. Calorimetric measurement of induction motor harmonic losses.

[6] Packard, H., 1996. HP 34401A Multimeter Users Guide.*Hewlett Packard Company*.

[7] Chen, T.C., Chen, J.S. and Tsai, C.C., 1991, May. Measurement of induction motor parameter identification. In *Instrumentation and Measurement Technology Conference, 1991. IMTC-91. Conference Record., 8th IEEE* (pp. 288-291). IEEE.

[8] Pyrhonen, J., Jokinen, T. and Hrabovcova, V., 2013. *Design of rotating electrical machines*. John Wiley Sons.

[9] Islam, M.J., Khang, H.V., Repo, A.K. and Arkkio, A., 2010. Eddy-current loss and temperature rise in the form-wound stator winding of an inverter-fed cage induction motor. *IEEE Transactions on Magnetics, 46(8)*, pp.3413-3416.

[10] Parekh, R., 2003. AC Induction Motor Fundamentals. *Microchip Technology Inc.*

[11] Zhang, D., Shi, J., Zhao, H. and Wu, T., 2017, October. Loss characteristic analysis of small and medium-sized induction motors fed by PWM inverter based on the experiment measurements. In *Industrial Electronics Society, IECON 2017-43rd Annual Conference of the IEEE* (pp. 2053-2058). IEEE.

[12] Aarniovuori, L., Rasilo, P., Niemelä, M. and Pyrhönen, J.J., 2016. Analysis of 37-kW converter-fed induction motor losses. *IEEE Transactions on Industrial Electronics, 63(9)*, pp.5357-5365.

[13] Pippuri, J. and Arkkio, A., 2008, September. Challenges in the segregation of losses in cage induction machines. In Electrical Machines, 2008. *ICEM 2008. 18th International Conference on* (pp. 1-5). IEEE.

[14] Szabados, B. and Mihalcea, A., 2002. Design and implementation of a calorimetric measurement facility for determining losses in electrical machines. *IEEE Transactions on Instrumentation and Measurement, 51(5)*, pp.902-907.

[15] Kepsu, M.M., 2015. Uncertainty of efficiency measurements in electric drives.

[16] Bucci, G., Ciancetta, F., Fiorucci, E. and Ometto, A., 2016. Uncertainty issues in direct and indirect efficiency determination for three-phase induction motors: remarks about the IEC 60034-2-1 standard. *IEEE Transactions on Instrumentation and Measurement, 65(12)*, pp.2701-2716.

[17] TECHNICAL NOTE IEC 60034-30-1 standard on efficiency classes for low voltage AC motors, https://library.e.abb.com/public/0451229996ff4b0786505fd9a4075645/9AKK107319%20EN%2005-2018_20848_ABB_Technical_note_IEC_60034_30_1.pdf, Accessed: 2018-11-21

[18] Nair, D., 2013. Calorimetric Power Loss Measurement of a Small Power Converter.

[19] Cao, W., Bradley, K.J., French, I., Zhang, J. and Zhang, H., 2006, September. A review of calorimetric application for accurate power loss measurement. In *Universities Power Engineering Conference, 2006. UPEC'06. Proceedings of the 41st International* (Vol. 2, pp. 550-554). IEEE.

[20] Bradley, K.J., Cao, W. and Arellano-Padilla, J., 2006. Evaluation of stray load loss in induction motors with a comparison of input-output and calorimetric methods. *IEEE Transactions on Energy Conversion, 21(3)*, pp.682-689.

[21] Zhang, H., Zanchetta, P., Gerada, C., Cao, W. and Bradley, K., 2010, November. Design of a calorimeter for induction machine efficiency measurement by CFD modeling. In *IECON 2010-36th Annual Conference on IEEE Industrial Electronics Society* (pp. 817-822). IEEE.

[22] Cao, W., Asher, G.M., Huang, X., Zhang, H., French, I., Zhang, J. and Short, M., 2010. Calorimeters and techniques used for power loss measurements in electrical machines. *IEEE instrumentation measurement magazine, 13(6).*

[23] Cao, W., Huang, X. and French, I., 2009. Design of a 300-kW calorimeter for electrical motor loss measurement. *IEEE Transactions on Instrumentation and Measurement, 58(7)*, pp.2365-2367.

[24] Kosonen, A., Aarniovuori, L., Ahola, J., Backman, J., Pyrhönen, J. and Niemelä, M., 2014. Loss definition of electric drives by a calorimetric system with data processing. *IEEE Transactions on Industrial Electronics, 61(8)*, pp.4432-4442.

[25] Jalilian, A., Gosbell, V.J., Perera, B.S.P. and Cooper, P.A.C.P., 1999. Double chamber calorimeter (DCC): A new approach to measure induction motor harmonic losses. *IEEE Transactions on Energy Conversion, 14(3)*, pp.680-685.

[26] Nair, D.G., Daryabin, S., Jannasch, S., Haavisto, A. and Arkkio, A., 2018, September. Design of Water-Cooled Calorimeter for Electric Motor's Power Loss Measurement. In *2018 XIII International Conference on Electrical Machines (ICEM)* (pp. 1142-1148). IEEE.

[27] ALICAT SCIENTIFIC Operating ManualPrecision Water Flow Meter Precision Water Flow Controller, https://documents.alicat.com/manuals/Liquid_Flow_Meter_Controller_Manual.pdf, Accessed: 2018-11-21

[28] Bonnett, A.H., 2000. Operating temperature considerations and performance characteristics for IEEE 841 motors. In Petroleum and Chemical Industry Conference, 2000. Record of Conference Papers. *Industry Applications Society 47th Annual* (pp. 77-89). IEEE.

[29] Steinmetz, J., Patel, S.C. and Zocholl, S.E., 2013, April. Stator thermal time constant. In *Industrial Commercial Power Systems Technical Conf (ICPS), 2013 IEEE/IAS 49th* (pp. 1-7). IEEE.

[30] Hughes, A. and Drury, W., 2013. Electric motors and drives: fundamentals, types and applications. Newnes.

[31] Rotating electrical machines- Part 2: Methods for determining losses and efficiency of rotating electrical machinery from test(excluding machines for traction vehicles) Measurement of losses by the calorimetric method. IEC 34-2, 1972.

[32] Pawlus, W., Van Khang, H. and Hansen, M.R., 2017. Temperature rise estimation of induction motor drives based on loadability curves to facilitate design of electric powertrains.*IEEE Transactions on Industrial Informatics, 13(3)*, pp.985-994.

[33] Zocholl, S.E. and Benmouyal, G., 2001, October. Using thermal limit curves to define thermal models of induction motors. In *28th Western Protective Relay Conference*.

[34] Zhang, H., Cao, W., Zanchetta, P. and Li, J., 2011, September. Thermal analysis of a balanced calorimeter for testing electrical machines. In *Energy Conversion Congress and Exposition (ECCE), 2011 IEEE* (pp. 429-432). IEEE.

[35] Yabiku, R., Fialho, R., Teran, L., Ramos, M.E. and Kawasaki, N., 2010. Use of thermal network on determining the temperature distribution inside electric motors in steady-state and dynamic conditions. *IEEE Transactions on Industry Applications, 46(5)*, pp.1787-1795.

[36] Vanhaelst, R., Kheir, A. and Czajka, J., 2016. A systematic analysis of the friction losses on bearings of modern turbocharger. *Combustion Engines, 55.*

[37] Cousseau, T., Graça, B., Campos, A. and Seabra, J., 2011. Friction torque in grease lubricated thrust ball bearings. *Tribology international, 44(5)*, pp.523-531.

[38] Rasilo, P., Ekstrom, J., Haavisto, A., Belahcen, A. and Arkkio, A., 2012. Calorimetric system for measurement of synchronous machine losses. *IET electric power applications, 6(5)*, pp.286-294.

Appendix

A Uncertainty in Power Measurement

If the heat capacity and water density are assumed constant, the uncertainty in balanced-water cooled calorimeter is due to the three factors:

First, the uncertainty of the temperature sensor of the inlet and outlet of the calorimeter. Second, the uncertainty in the water flow measurement, and third, the difference of the heat-leakage during the balance test and the actual test. If the water heat capacity and density are assumed constant, the coolant power is expressed as a function of the inlet and outlet temperatures and the water flow rate.

$$P_{\mathrm{W}} = k\dot{V}\Delta T = k\dot{V}(T_{\mathrm{o}} - T_{\mathrm{i}}) = f(\dot{V}, T_{\mathrm{o}}, T_{\mathrm{i}}) \tag{A1}$$

Where the term k represents the constant value of the product of the water heat capacity and density, and f indicates the non-linear relationship of the input parameter $\dot{V}$,T_{i} and T_{o}. For a variable y with $\pm\alpha$ uniform distribution of error, the standard uncertainty is defined as

$$u(y) = \frac{\alpha}{\sqrt{3}} \tag{A2}$$

Table A1 shows the instruments errors and their corresponded standard uncertainties when the measued coolant power is 2.643 kW and the tested motor's torque is 201.88 Nm. The combined uncertainty of the coolant power can be calculated as the following equations:

$$u_{\mathrm{c}}(\Delta T) = \sqrt{u(T_{\mathrm{in}})^2 + u(T_{\mathrm{o}})^2} = 0.1774^{\circ}\mathrm{C}$$

$$\frac{u(P_{\mathrm{W}})}{P_{\mathrm{W}}} = \sqrt{(\frac{u(\Delta T)}{\Delta T})^2 + (\frac{u(\dot{V})}{\dot{V}})^2} = \frac{u(P_{\mathrm{W}})}{2.643\mathrm{kW}} = 0.024 \tag{A4}$$

$$u(P_{\mathrm{W}}) = \pm 63.43\mathrm{W} = 2.4\% \tag{A5}$$

If the difference of the heat-leakage between the balance test and actual test, and the uncertainty of the power loss measurement of the reference heater through the power analyser are neglected, the uncertainty of the balance water-cooled calorimeter is 2.4%, and the expanded uncertainty is 4.8%, when the torque of the test motor is 201.88 Nm close to the rated torque.

The difference of the heat-leakage during the actual test and the balance test is due to the different placement of the reference heater and the tested motor[38]. In addition, the reference heater and the test motor have different surface area, and as a result they have different heat distribution which brings about the difference in the heat-leakage.

Table A1: Error of measurement

variable x_{i}	Estimate	error $\pm\alpha$	Standard Uncertainty $\mathrm{u}(\mathrm{x_i})$
Inlet Water Temperature T_{i}	13.2°C	$\pm(0.15 + 0.002T_{\mathrm{i}})$°C	0.1018°C
Outlet Water Temperature T_{o}	20.7°C	$\pm(0.15 + 0.002T_{\mathrm{o}})$°C	0.1105°C
Water Flow $\dot{V}$	$5\frac{\mathrm{L}}{\mathrm{min}}$	$\pm 0.02\frac{\mathrm{L}}{\mathrm{min}}$	$0.0115\frac{\mathrm{L}}{\mathrm{min}}$